Supporting Information for

Balancing Enthalpy and Entropy Changes in Inhibitors binding to the Prostate-Specific Membrane Antigen (PSMA)

Yuqing Xiong [a], Xinlin Wang [b], Mengchao Cui [a, b,*], Yajun Liu [a,*], Beibei Wang [a,*]

[a] Center for Advanced Materials Research, Beijing Normal University at Zhuhai, Zhuhai 519087, China;

[b] Key Laboratory of Radiopharmaceuticals, Ministry of Education, Beijing Normal University, Beijing 100875, China.

* Corresponding authors: Mengchao Cui: cmc@bnu.edu.cn; Yajun Liu: yajun.liu@bnu.edu.cn; Beibei Wang: bbwang@bnu.edu.cn.

Supplementary Methods and Materials

Synthesis

*Synthesis of Compound **2**.* To the suspension of **1** (1.00 g, 7.24 mmol) in acetonitrile (30 mL) was added *N*,*N*-Diisopropylethylamine (3.0 mL). The reaction mixture was stirred at room temperature under SO_2F_2 for 12 h. The solvent was removed by evaporation in vacuum. The residue was added to 15 mL of ethyl acetate and ultrasonically vibrated for 5 min. The solid was collected by filtration and washed with ethyl acetate to to give **2** as a white solid, which was used for the next step without further purification.

*Synthesis of Compound **3**.* Crude compound **2** (1.54 g, ~6.99 mmol) was suspended in CH_2Cl_2 (30 mL), and the 2,3,5,6-tetrafluorophenol (1.39 g, 8.37 mmol), N,N-Dicyclohexylcarbodiimide (1.44 g, 6.99 mmol) was added. The reaction mixture was stirred at room temperature for 4 h. The solvent was removed by evaporation in vacuum, and the residue was purified by silica gel column chromatography to give **3** as a white solid (1.88 g, ~73%). ^{1}H NMR (600 MHz, $CDCl_3$) δ 8.29 (m, 1H), 8.18 (s, 1H), 7.71 - 7.70 (m, 2H), 7.09 (m, 1H). ^{19}F NMR (565 MHz, $CDCl_3$) δ 38.74, 138.31, 152.43.

*Synthesis of Compound **4**.* Compound **3** (814 mg, 2.21 mmol), di-tert-butyl (((*S*)-6-amino-1-(tert-butoxy)-1-oxohexan-2-yl)carbamoyl)-*L*-glutamate (1.29 g, 2.65 mmol), and triethylamine (650 μL) was dissolved in CH_2Cl_2. The reaction mixture was stirred at room temperature for 3 h. The solvent was removed by evaporation in vacuum, and the residue was purified by silica gel column chromatography to give **4** as a white solid (1.20 g, 80%). ^{1}H NMR (400 MHz, DMSO–d_6) δ 8.67 (t, J = 5.4 Hz, 1H), 7.98 (d, J = 8.5 Hz, 1H), 7.97 (s, 1H), 7.75 (d, J = 8.7 Hz, 1H), 7.69 (t, J = 7.9 Hz, 1H), 6.28 (t, J = 7.8 Hz, 2H), 4.04 - 3.97 (m, 2H), 3.30 - 3.25 (m, 2H), 2.24 - 2.17 (m, 2H), 1.90 - 1.82 (m, 1H), 1.70 - 1.61 (s, 2H), 1.57 - 1.50 (m, 3H), 1.41 - 1.39 (m, 2H), 1.38 - 1.37 (m, 18H), 1.35 (s, 9H). ^{19}F NMR (565 MHz, DMSO–d_6) δ 39.16.

*Synthesis of Compound **M01**.* Compound **4** (1.14 g, 1.65 mmol) was dissolved in 9 mL CH_2Cl_2, and 9 mL trifluoroacetic acid was added. The reaction mixture was stirred at room temperature for 4 h. Then, the solvent was evaporated under vacuum, and ethyl acetate (10 mL) was added. The precipitate was isolated by centrifugation, washed with ethyl acetateand petroleum ether three times, and finally dried to give the final product as white solid (793 mg, 92%). ^{1}H NMR (400 MHz,

DMSO–d_6) δ 12.41 (brs, 3H), 8.68 (s, 1H), 7.98 (s, 2H), 7.77 (d, J = 7.1 Hz, 1H), 7.69 (t, J = 7.1 Hz, 1H), 6.31 (s, 2H), 4.08 (m, 2H), 3.26 (m, 2H), 2.24 (m, 2H), 1.91 (m, 1H), 1.70 (m, 2H), 1.54 (s, 3H), 1.34 (m, 2H). ^{19}F NMR (376 MHz, DMSO–d_6) δ 39.02. HRMS: m/z calculated for $[C_{19}H_{24}O_{11}N_3FNaS]^+$ 544.1008; found 544.1009.

*Synthesis of Compound **5**.* Following the synthesis procedure of compound **4** using the corresponding amino compound, di-tert-butyl (((*S*)-6-amino-1-(tert-butoxy)-1-oxohexan-2-yl)carbamoyl)-*D*-glutamate. The final compound **5** was obtained as a white solid (300 mg, 83%). ^{1}H NMR (400 MHz, $CDCl_3$) δ 7.95 – 7.86 (m, 2H), 7.55 (t, J = 8.0 Hz, 1H), 7.46 (dd, J = 8.2, 2.5 Hz, 1H), 7.05 (t, J = 5.4 Hz, 1H), 5.51 – 5.20 (m, 2H), 4.32 (dd, J = 8.5, 4.3 Hz, 1H), 4.25 (dd, J = 8.0, 5.2 Hz, 1H), 3.55 – 3.36 (m, 2H), 2.28 – 2.12 (m, 2H), 2.01 – 1.93 (m, 1H), 1.87 – 1.77 (m, 2H), 1.73 – 1.59 (m, 3H), 1.52 – 1.42 (m, 20H), 1.42 (s, 9H). ^{19}F NMR (376 MHz, Chloroform-d) δ 38.33.

*Synthesis of Compound **M02**.* Following the synthesis procedure of compound **M01**. The final compound **M02** was obtained as a white solid (210 mg, 90%). ^{1}H NMR (600 MHz, DMSO-d_6) δ 12.44 (s, 3H), 8.68 (t, J = 5.7 Hz, 1H), 8.02 – 7.94 (m, 2H), 7.77 (d, J = 8.3 Hz, 1H), 7.70 (t, J = 8.1 Hz, 1H), 6.37 (dd, J = 8.3, 3.7 Hz, 2H), 4.14 – 4.04 (m, 2H), 3.26 (q, J = 6.8 Hz, 2H), 2.27 – 2.15 (m, 2H), 1.94 – 1.85 (m, 1H), 1.75 – 1.63 (m, 2H), 1.59 – 1.48 (m, 3H), 1.37 – 1.27 (m, 2H). ^{19}F NMR (565 MHz, DMSO-d6) δ 39.17.

Synthesis of Compound 7. To the suspension of **6** (2.00 g, 10.98 mmol) in acetonitrile (50 mL) was added *N*,*N*-Diisopropylethylamine (8.0 mL). The reaction mixture was stirred at room temperature under SO_2F_2 for 12 h. The solvent was removed by evaporation in vacuum. The residue was added to 30 mL of ethyl acetate and ultrasonically vibrated for 5 min. The mixture was filtrated and the solution was washed by 10 mL H_2O twice. The organic layers were dried over $MgSO_4$ and concentrated under vacuum to give **7** as a brown oil, which was used for the next step without further purification.

*Synthesis of Compound **8**.* Following the synthesis procedure of compound **3**. The final compound **8** was obtained as a white solid (1.0 g, ~56%). ^{1}H NMR (600 MHz, $CDCl_3$) δ 9.08 (d, J = 0.9 Hz, 1H), 8.49 (s, 2H), 7.18 - 7.05 (m, 2H). ^{19}F NMR (565 MHz, $CDCl_3$) δ 39.77, 137.81, 152.15.

*Synthesis of Compound **9***. Following the synthesis procedure of compound **4**. The final compound **9** was obtained as a white solid (680 mg, 75%). ^{1}H NMR (400 MHz, $CDCl_3$) δ 8.54 (s, 1H), 8.12 (s, 2H), 7.85 (s, 2H), 5.87 (brs, 4H), 4.30 (dd, J = 8.2, 3.9 Hz, 2H), 4.18 (dd, J = 8.2, 5.1 Hz, 2H), 3.46 (s, 2H), 3.45 (s, 2H), 2.31 - 2.26 (m, 4H), 2.01 - 1.96 (m, 2H), 1.88 - 1.77 (m, 4H), 1.66 - 1.59 (m, 6H), 1.50 - 1.44 (m, 4H), 1.42 (s, 36H), 1.37 (s, 18H). ^{19}F NMR (565 MHz, $CDCl_3$) δ 39.06.

*Synthesis of Compound **D01***. Following the synthesis procedure of compound **M01**. The final compound **D01** was obtained as a white solid (593 mg, 90%). ^{1}H NMR (600 MHz, DMSO–d_6) δ 12.39 (brs, 6H), 8.78 (t, J = 4.9 Hz, 2H), 8.45 (s, 1H), 8.13 (s, 2H), 6.31 (t, J = 8.3 Hz, 4H), 4.08 (m, 4H), 3.28 (m, 2H), 3.27 (m, 2H), 2.29 - 2.19 (m, 4H), 1.94 - 1.89 (m, 2H), 1.74 - 1.66 (m, 4H), 1.58 - 1.54 (m, 6H), 1.39 - 1.34 (m, 4H). ^{19}F NMR (565 MHz, DMSO–d_6) δ 39.83. HRMS: m/z calculated for $[C_{32}H_{43}O_{19}N_6FNaS]^+$ 889.2180; found 889.2180.

*Synthesis of Compound **10***. Following the synthesis procedure of compound **5**. The final compound **10** was obtained as a white solid (600 mg, 83%). ^{1}H NMR (600 MHz, $CDCl_3$) δ 8.34 (s, 1H), 8.04 (s, 2H), 7.91 - 7.81 (m, 2H), 6.04 - 5.79 (m, 4H), 4.33 - 4.22 (m, 2H), 4.19 – 4.14 (m, 2H), 3.46 - 3.37 (m, 4H), 2.22 - 2.15 (m, 4H), 1.97 - 1.89 (m, 2H), 1.81 - 1.74 (m, 4H), 1.67 - 1.60 (m, 6H), 1.43 - 1.38 (m, 56H). ^{19}F NMR (565 MHz, $CDCl_3$) δ 39.05.

*Synthesis of Compound **D02***. Following the synthesis procedure of compound **M01**. The final compound **D02** was obtained as a white solid (450 mg, 86%). ^{1}H NMR (600 MHz, DMSO- d_6) δ 12.65 - 12.26 (m, 5H), 8.79 (t, J = 5.5 Hz, 2H), 8.45 (s, 1H), 8.13 (s, 2H), 6.37 (d, J = 8.2 Hz, 4H), 4.10 (dq, J = 14.4, 7.4 Hz, 4H), 3.28 - 3.25 (m, 4H), 2.27 - 2.15 (m, 4H), 1.92 - 1.85 (m, 2H), 1.74 - 1.64 (m, 4H), 1.59 - 1.52 (m, 6H), 1.36 - 1.29 (m, 4H). ^{19}F NMR (565 MHz, DMSO-d_6) δ 39.85.

In Vitro Inhibition Assay

PSMA inhibitory activity was determined using a modification of the N-acetylated-α-linked acidic dipeptidase (NAALADase) assay. Briefly, recombinant human PSMA protein (human PSMA/FOLH1 protein, 0.44 μg/mL, 50 μL) was incubated with the inhibitor (4 × 10−11 to 4 × 10−4 M, 25 μL) in the presence of 160 μM N-acetylaspartylglutamate (NAAG) (25 μL) in HEPES buffer at 37 °C for 60 min. Glutamate released by NAAG hydrolysis was measured by incubating with an

OPA (ortho-phthaldialdehyde) working solution for 3 min, avoiding light. Fluorescence was measured by a plate reader with excitation at 350 nm and emission at 450 nm. Semilog plots reflected the inhibition curve, and IC50 values were determined at the concentration where enzyme activity was inhibited by 50%. Enzyme inhibitory constants (Ki values) were generated through Cheng−Prusoff conversion (GraphPad Prism 8.3.0). Assays were performed in triplicate.

Supplementary characterization: NMR and MS Spectra of Compounds.

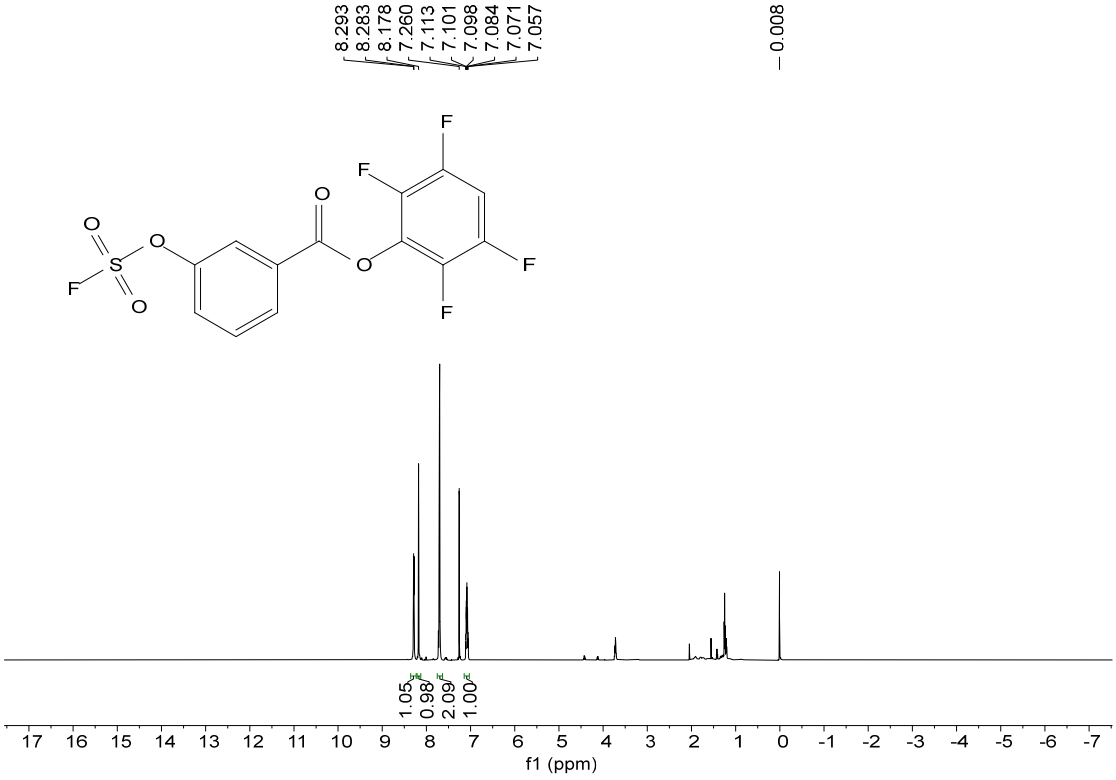

^{1}H -NMR spectrum of compound **3** in $CDCl_3$.

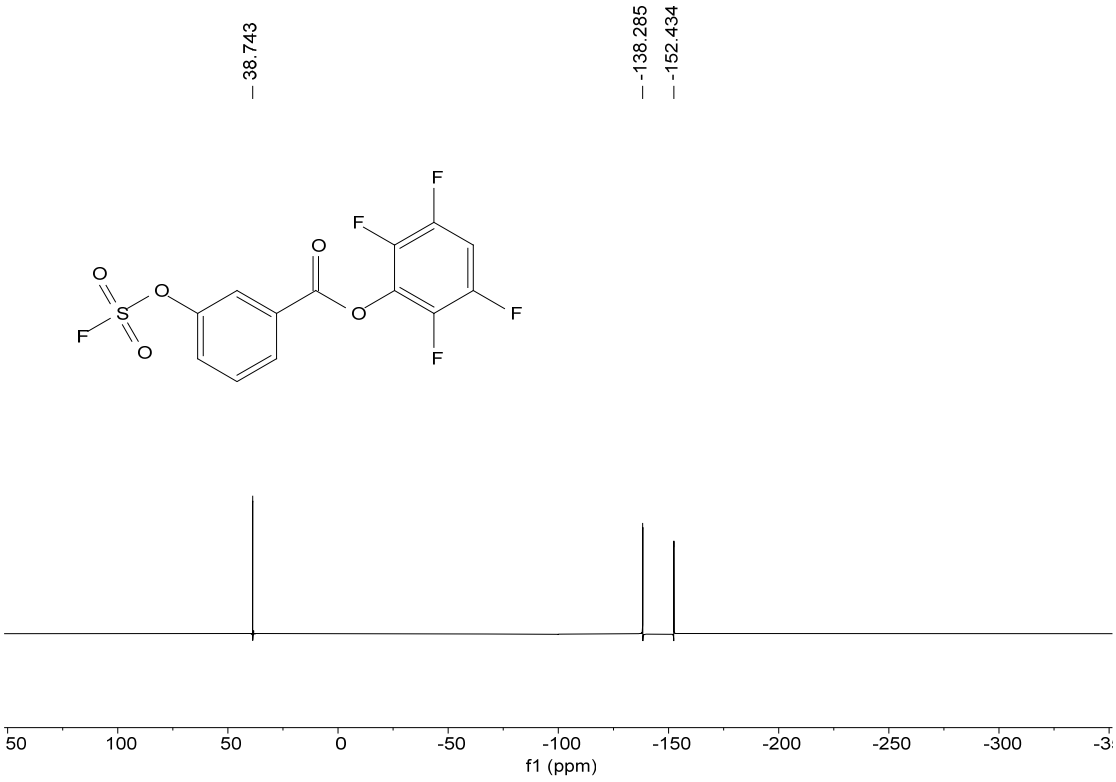

^{19}F -NMR spectrum of compound **3** in $CDCl_3$.

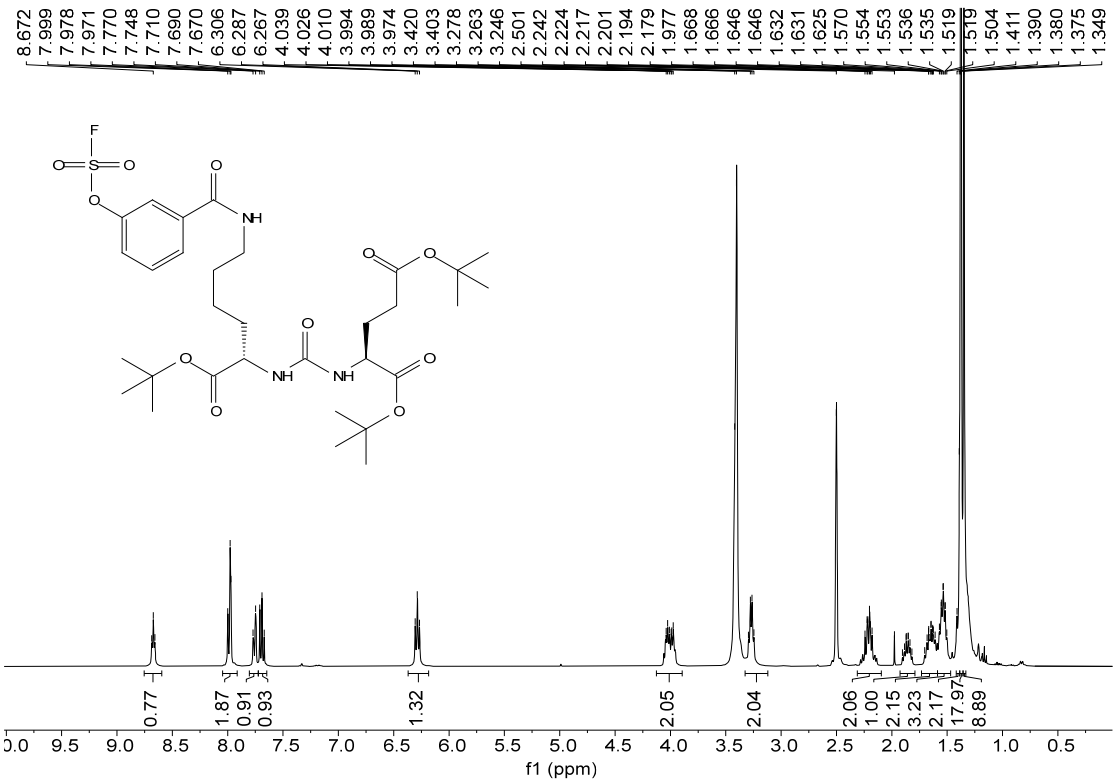

^{1}H -NMR spectrum of compound **4** in DMSO.

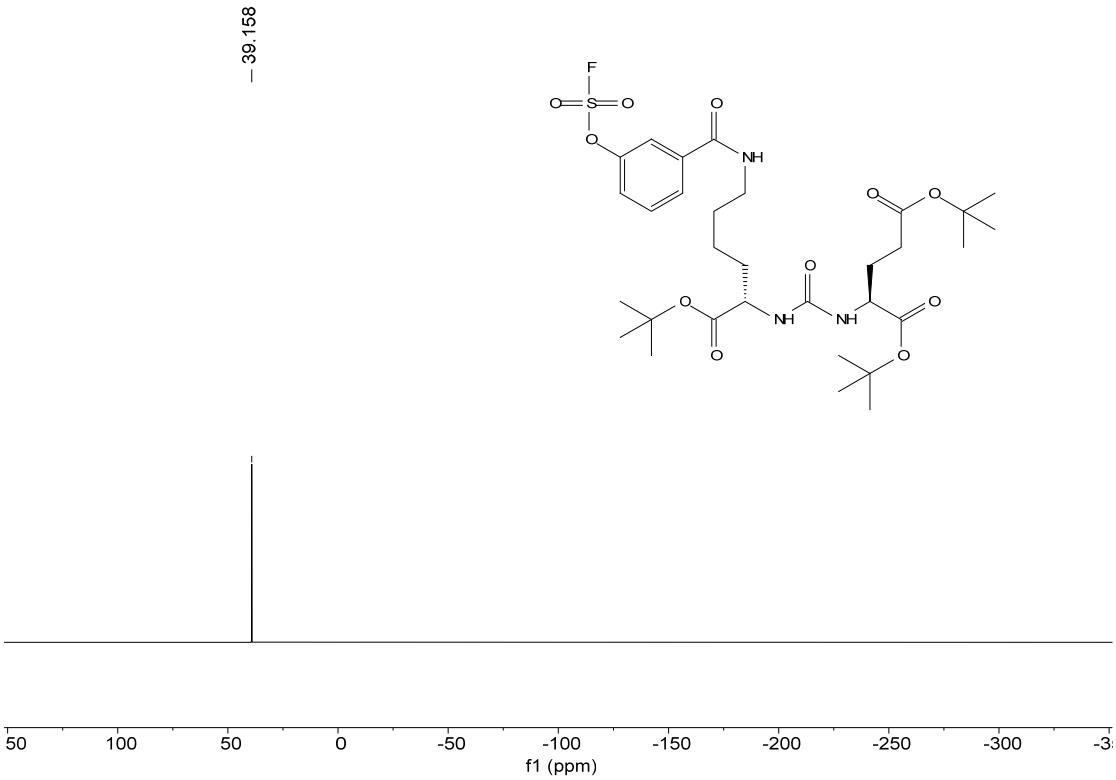

^{19}F -NMR spectrum of compound **4** in DMSO.

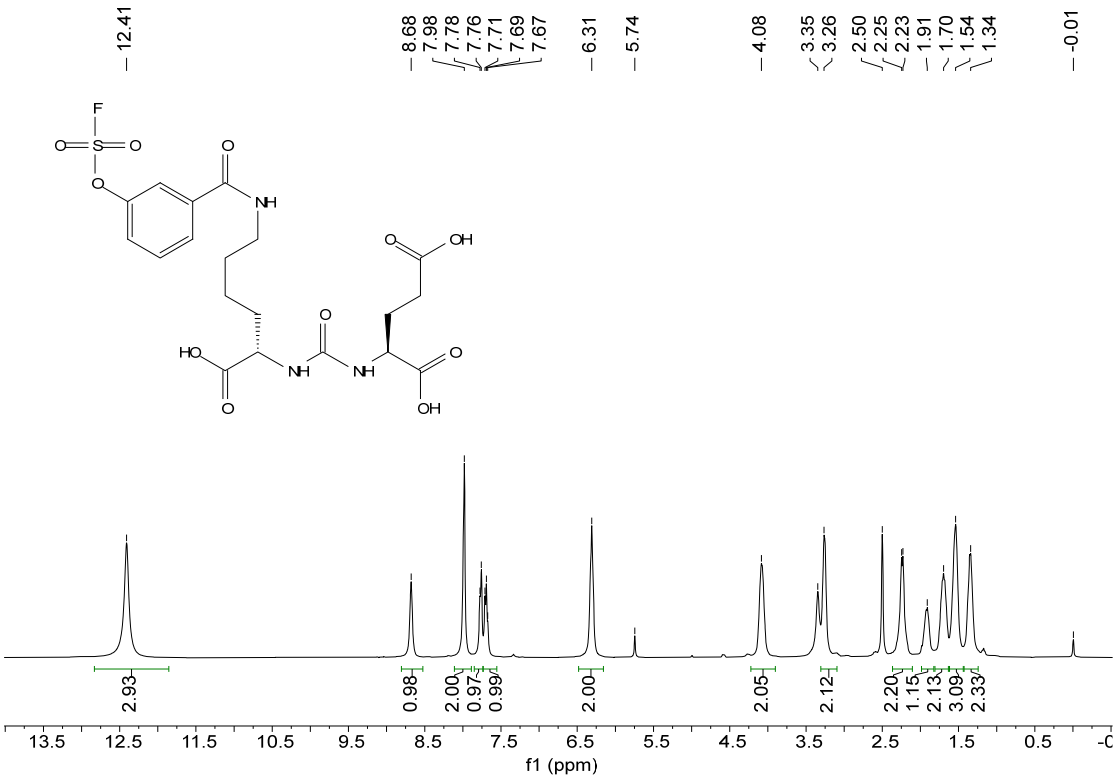

^{1}H -NMR spectrum of compound **M01** in DMSO.

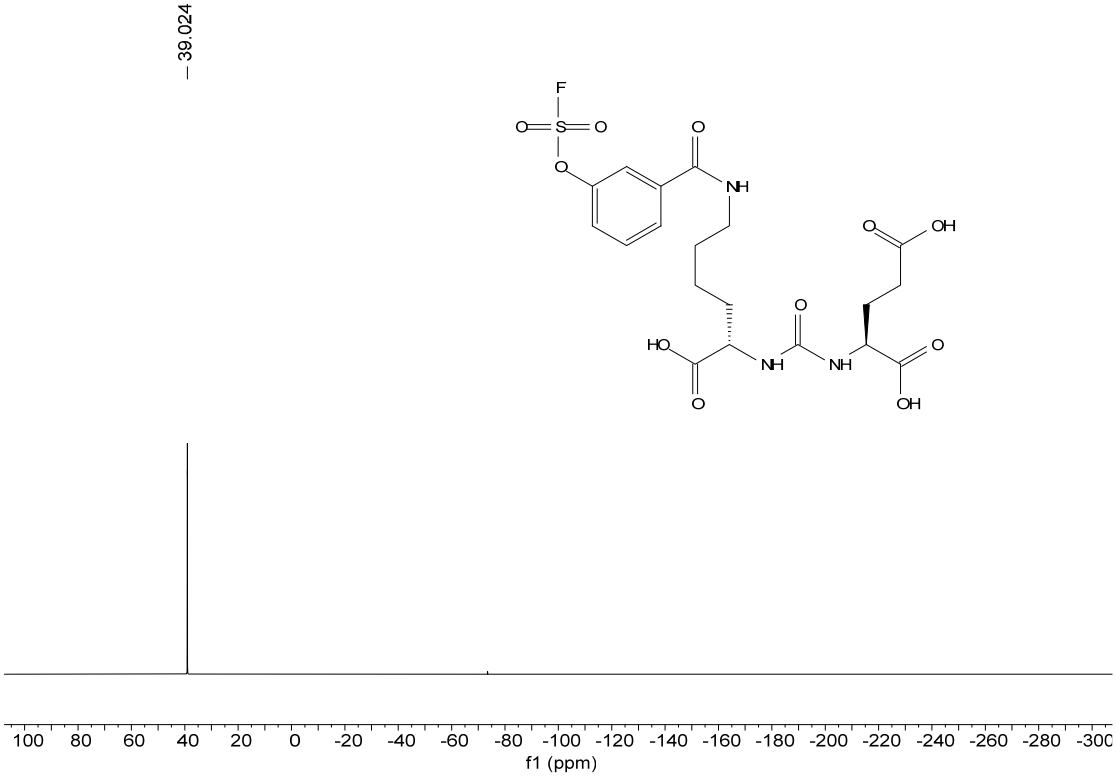

^{19}F -NMR spectrum of compound **M01** in DMSO.

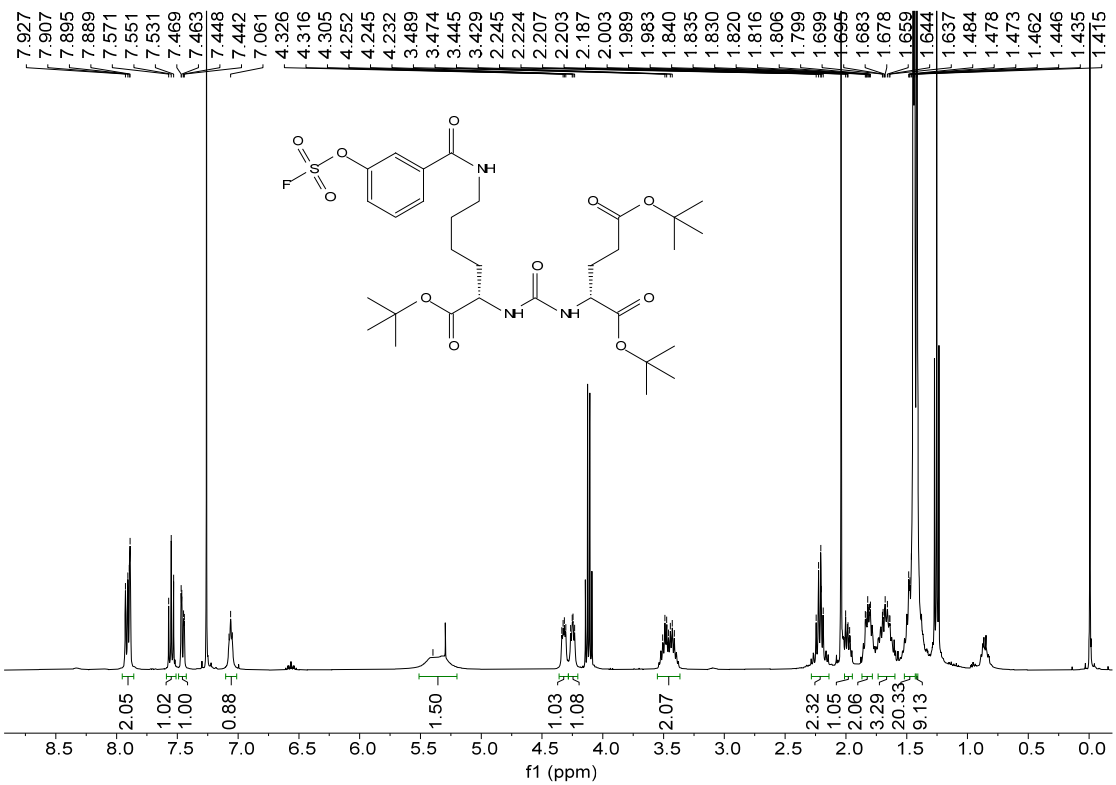

^{1}H -NMR spectrum of compound **5** in $CDCl_3$.

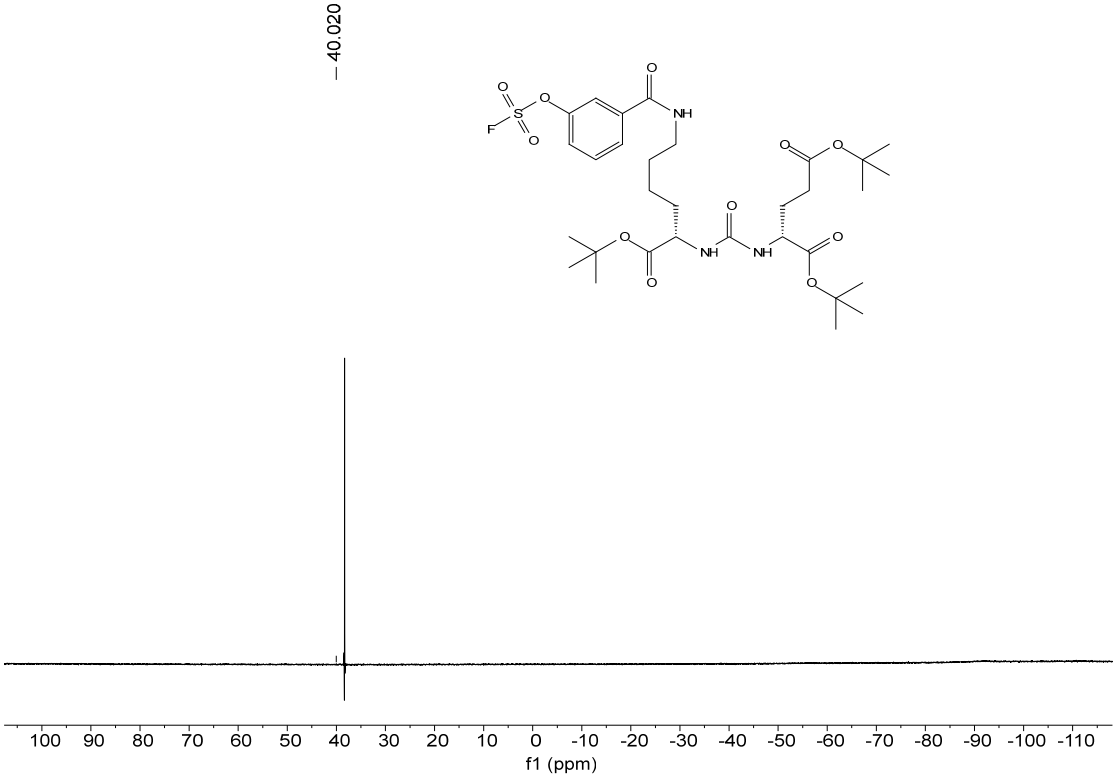

^{19}H -NMR spectrum of compound **5** in $CDCl_3$.

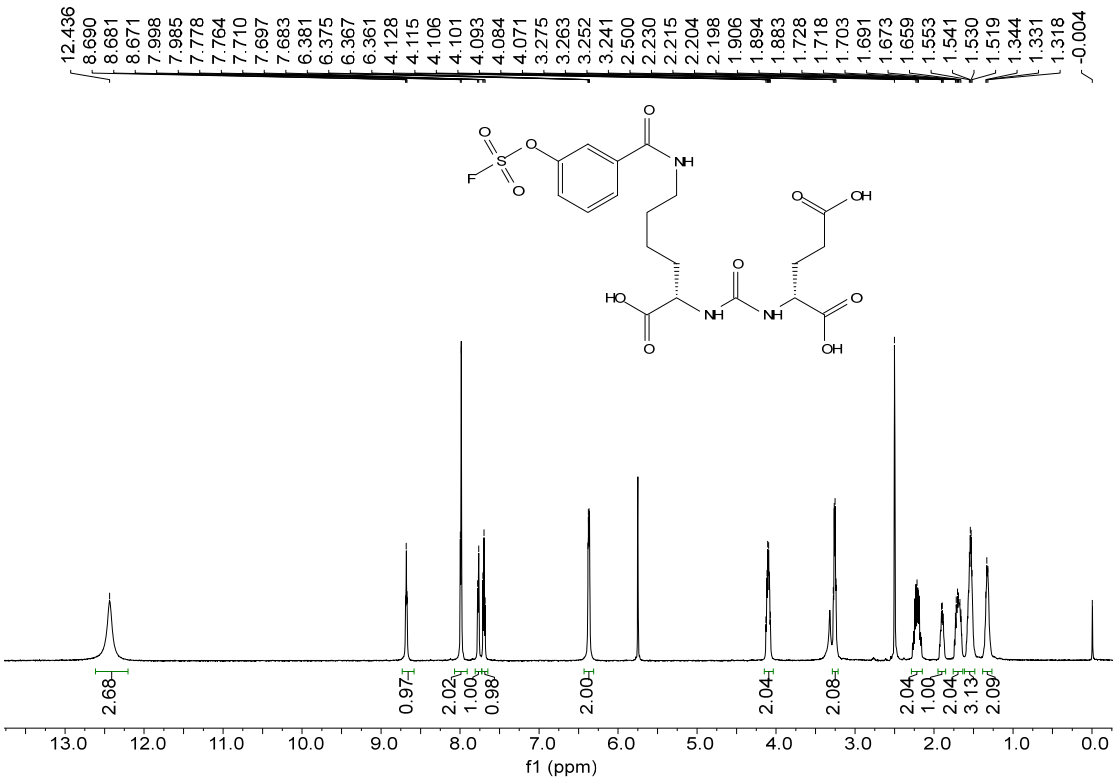

^{1}H -NMR spectrum of compound **M02** in DMSO.

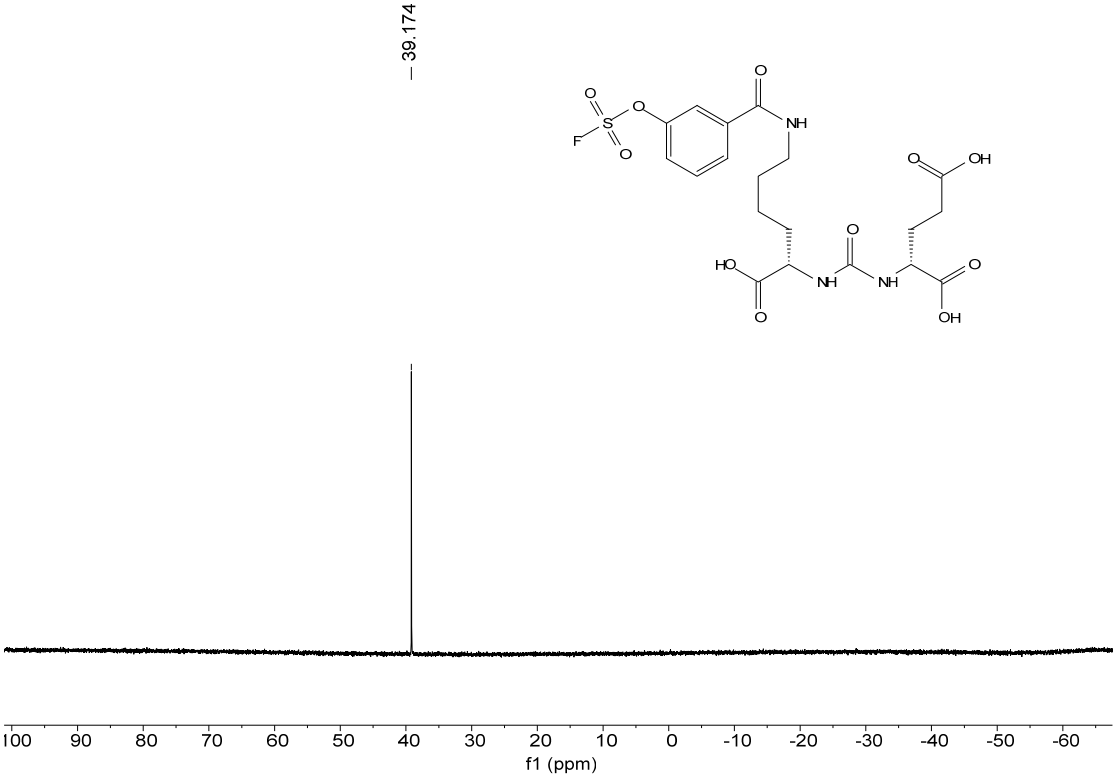

^{19}F -NMR spectrum of compound **M02** in DMSO.

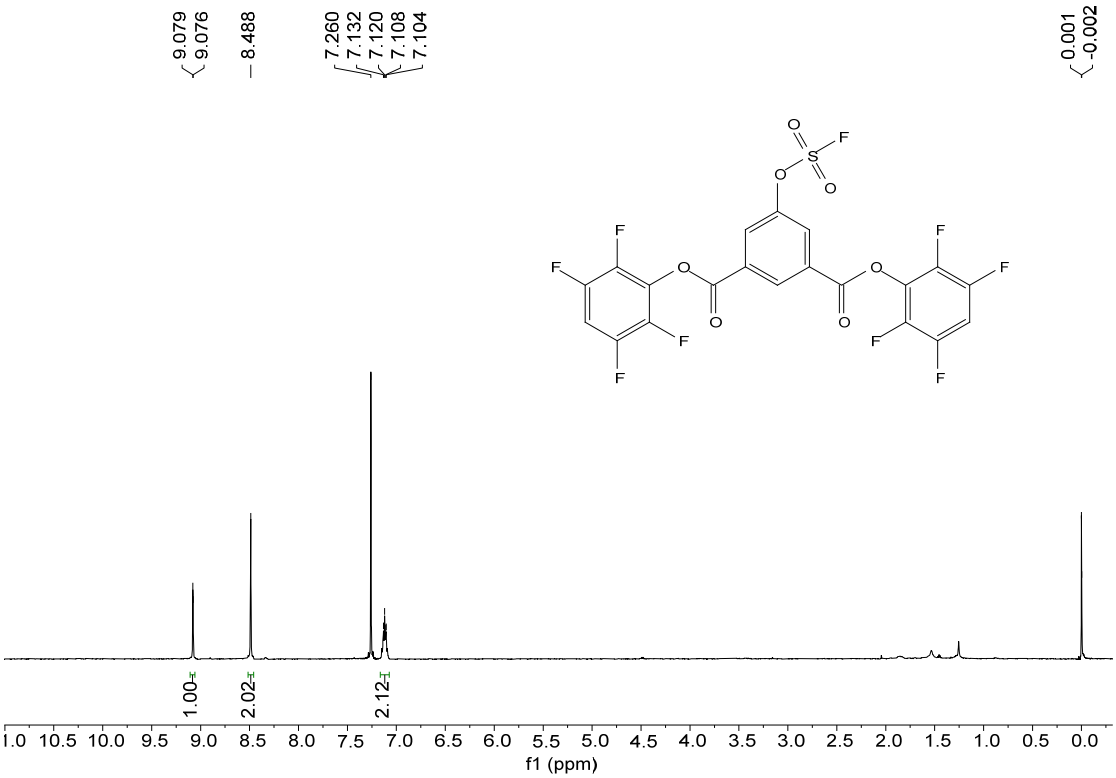

^{1}H -NMR spectrum of compound **8** in $CDCl_3$.

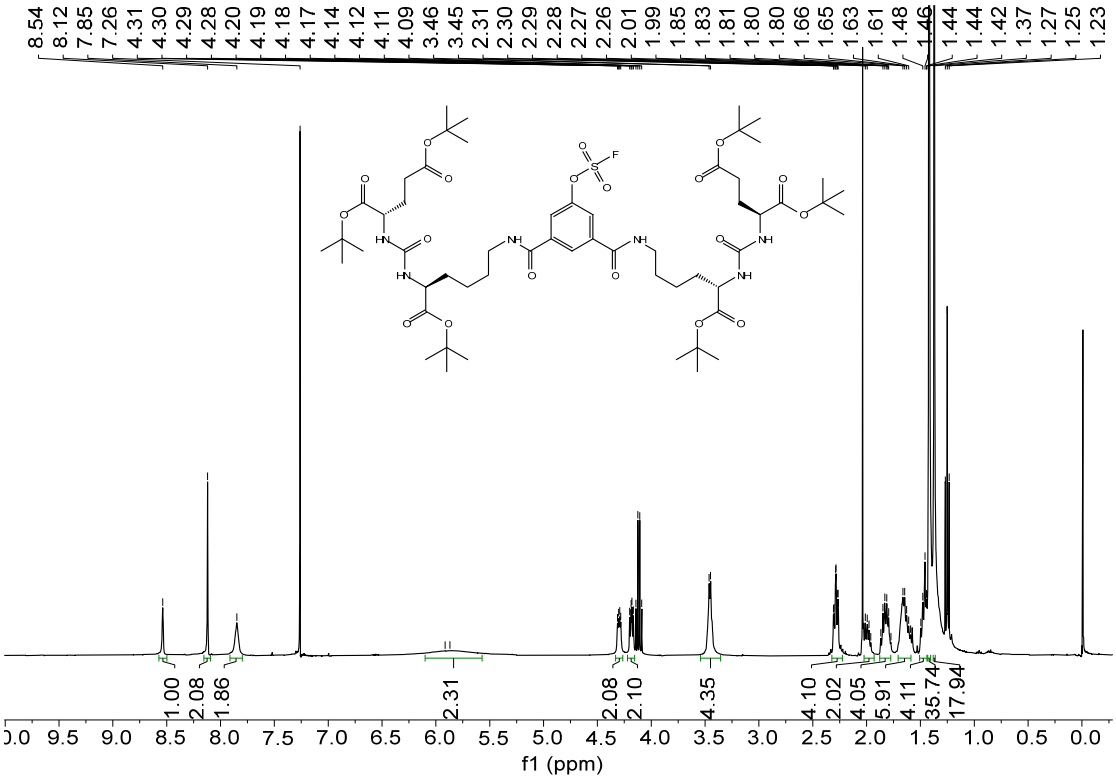

^{1}H -NMR spectrum of compound **9** in DMSO.

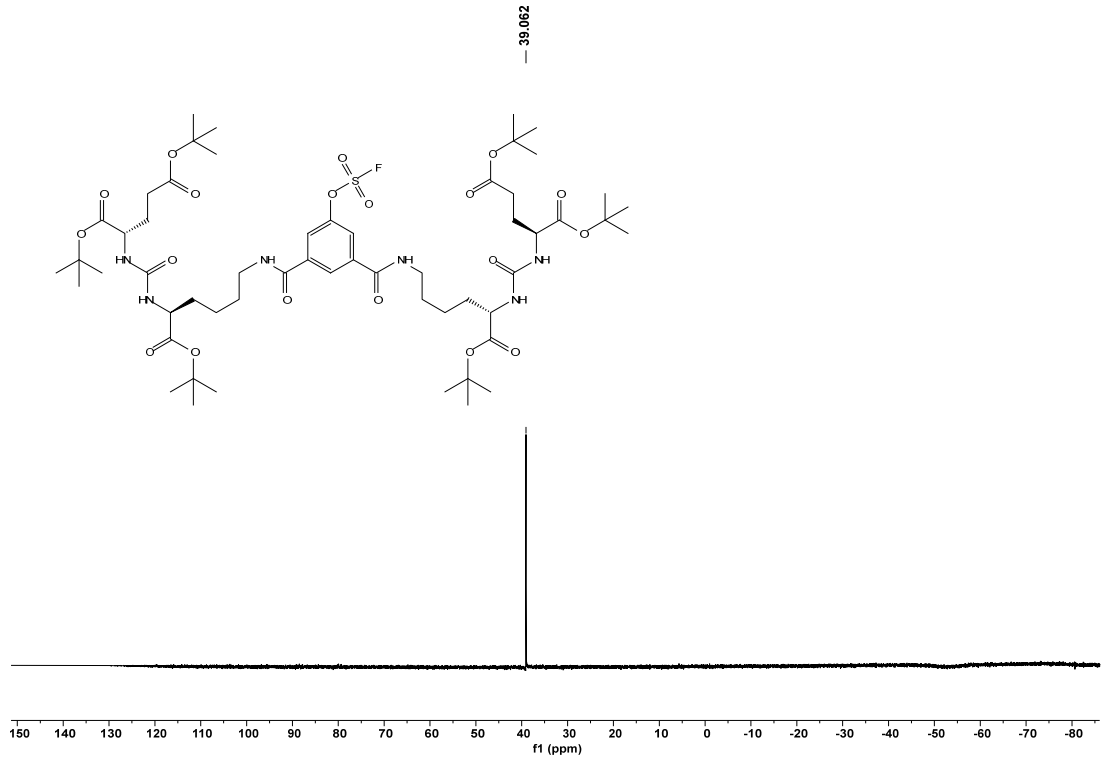

^{19}F -NMR spectrum of compound **9** in DMSO.

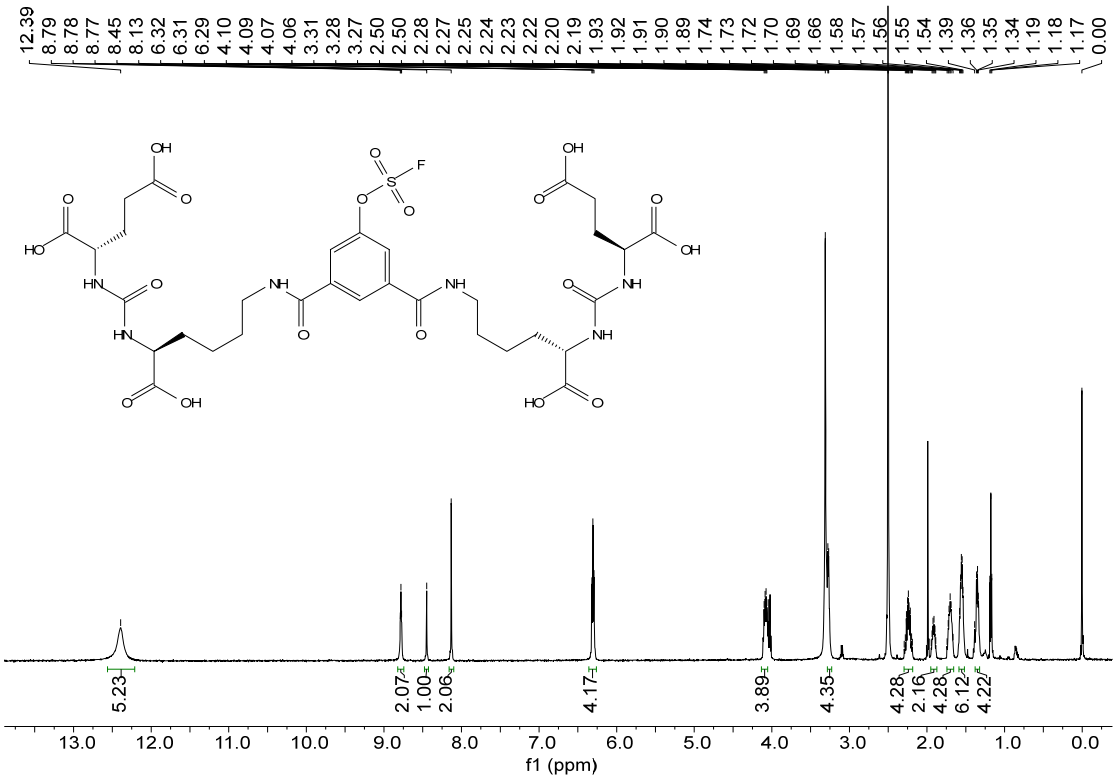

^{1}H -NMR spectrum of compound **D01** in DMSO.

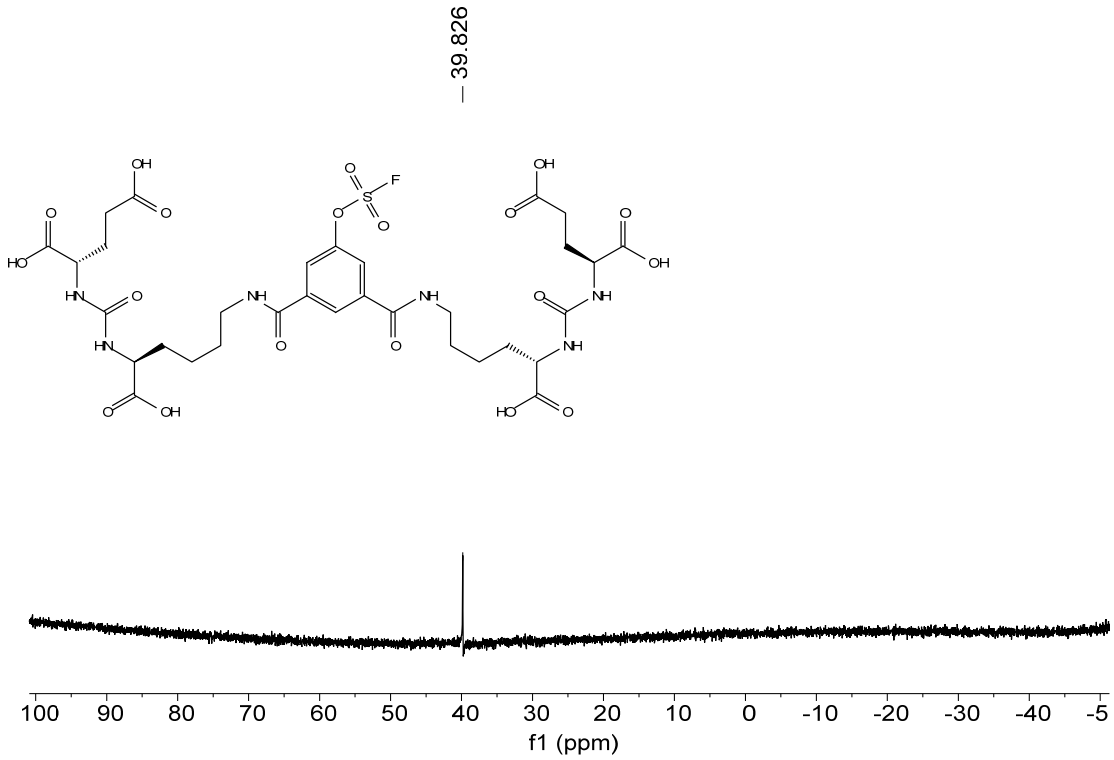

^{19}F -NMR spectrum of compound **D01** in DMSO.

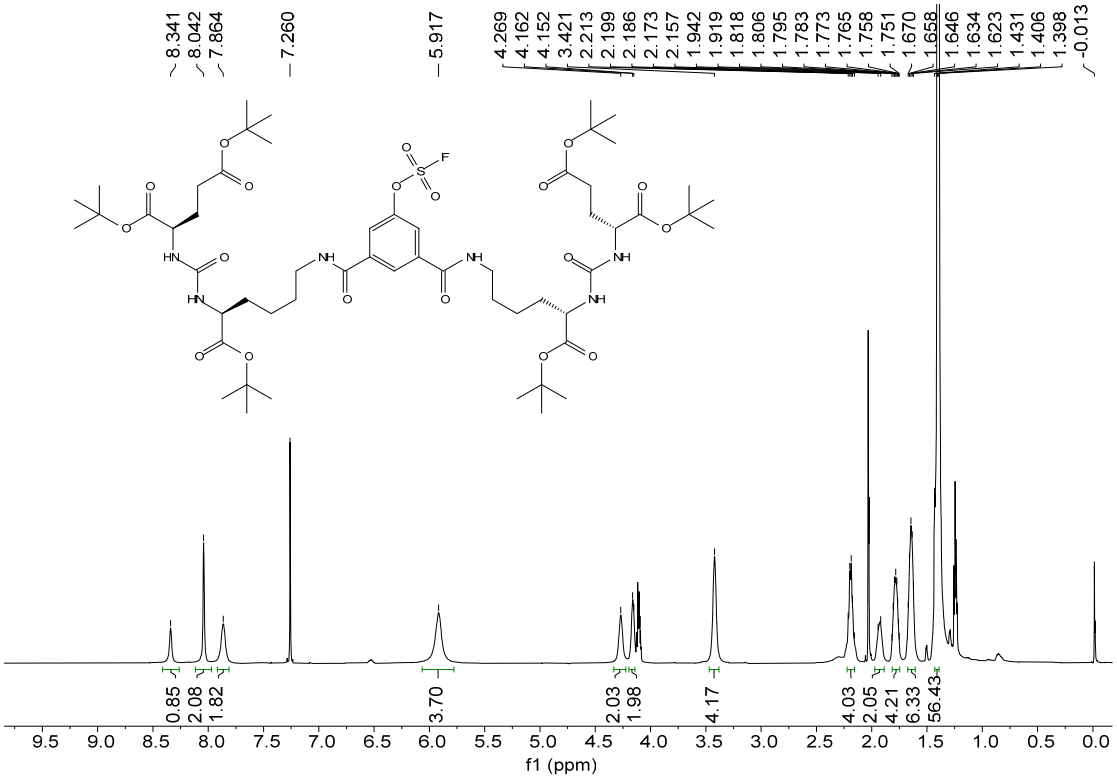

^{1}H -NMR spectrum of compound **10** in $CDCl_3$.

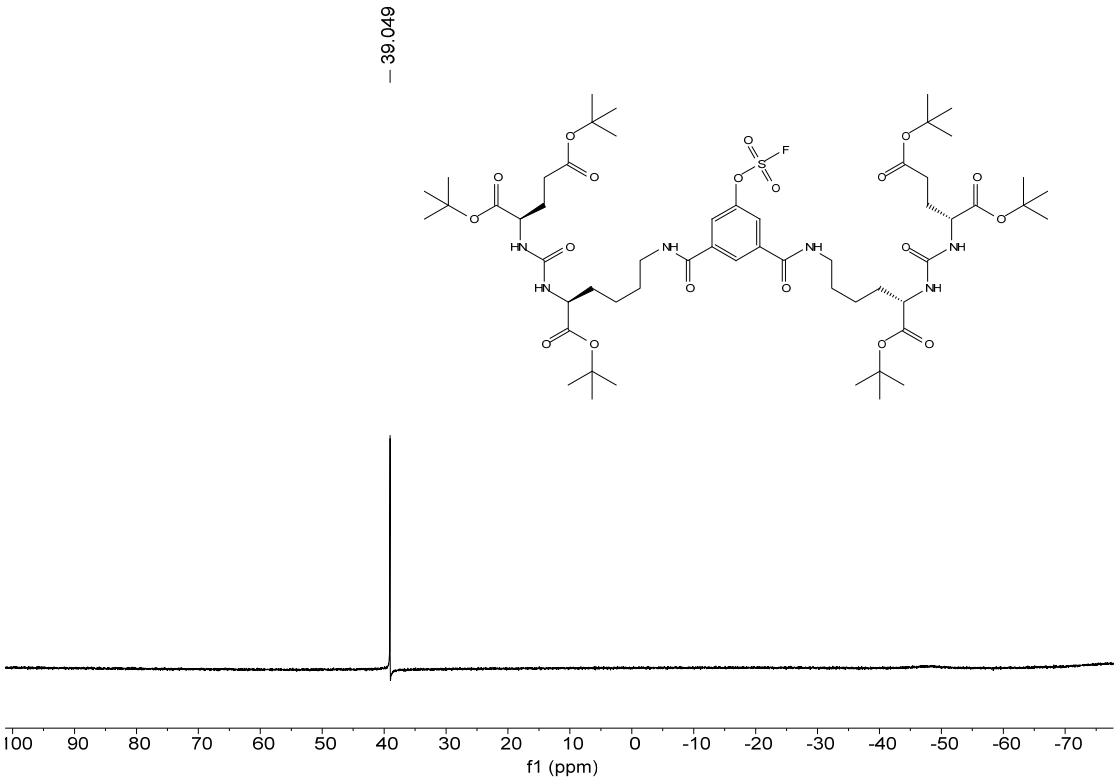

^{19}F -NMR spectrum of compound **10** in $CDCl_3$.

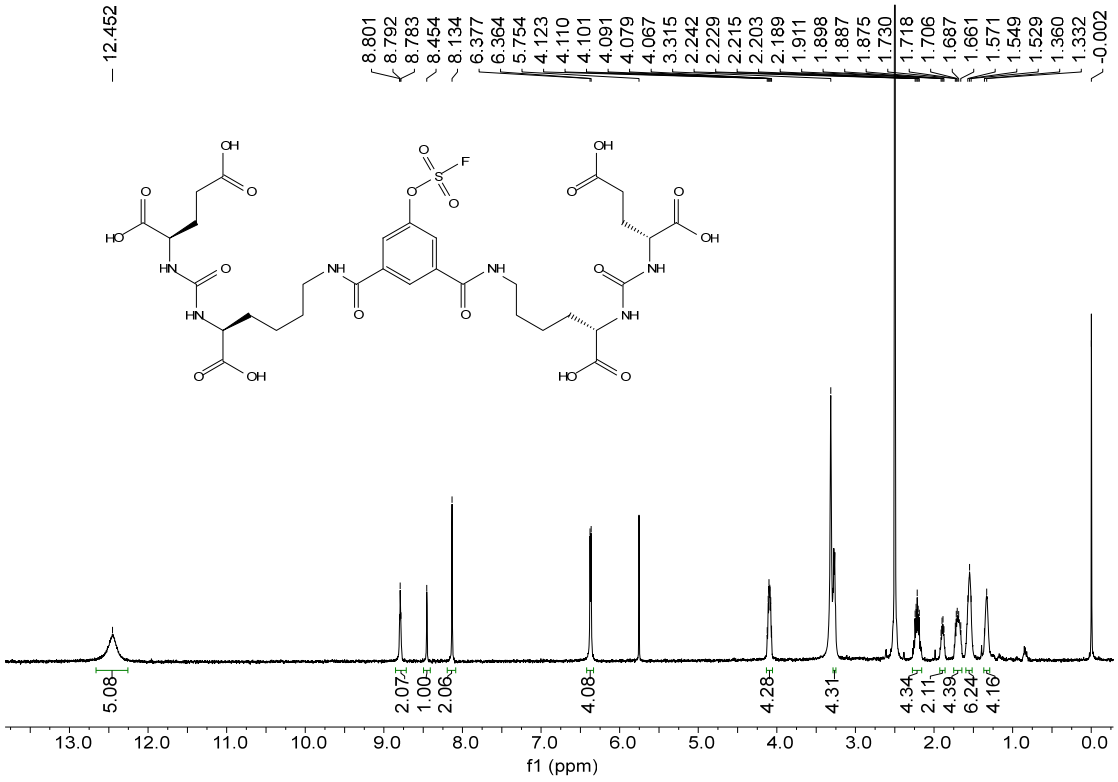

^{1}H -NMR spectrum of compound **D02** in DMSO.

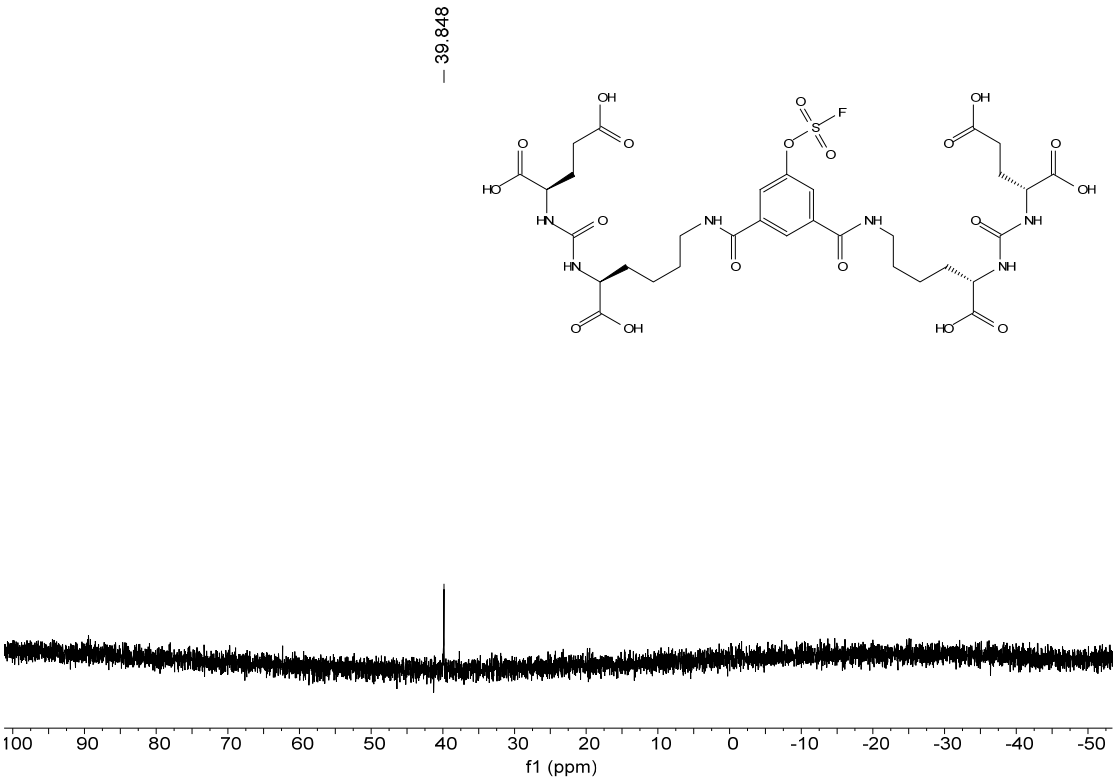

^{19}F -NMR spectrum of compound **D02** in DMSO.

Supplementary figures and tables:

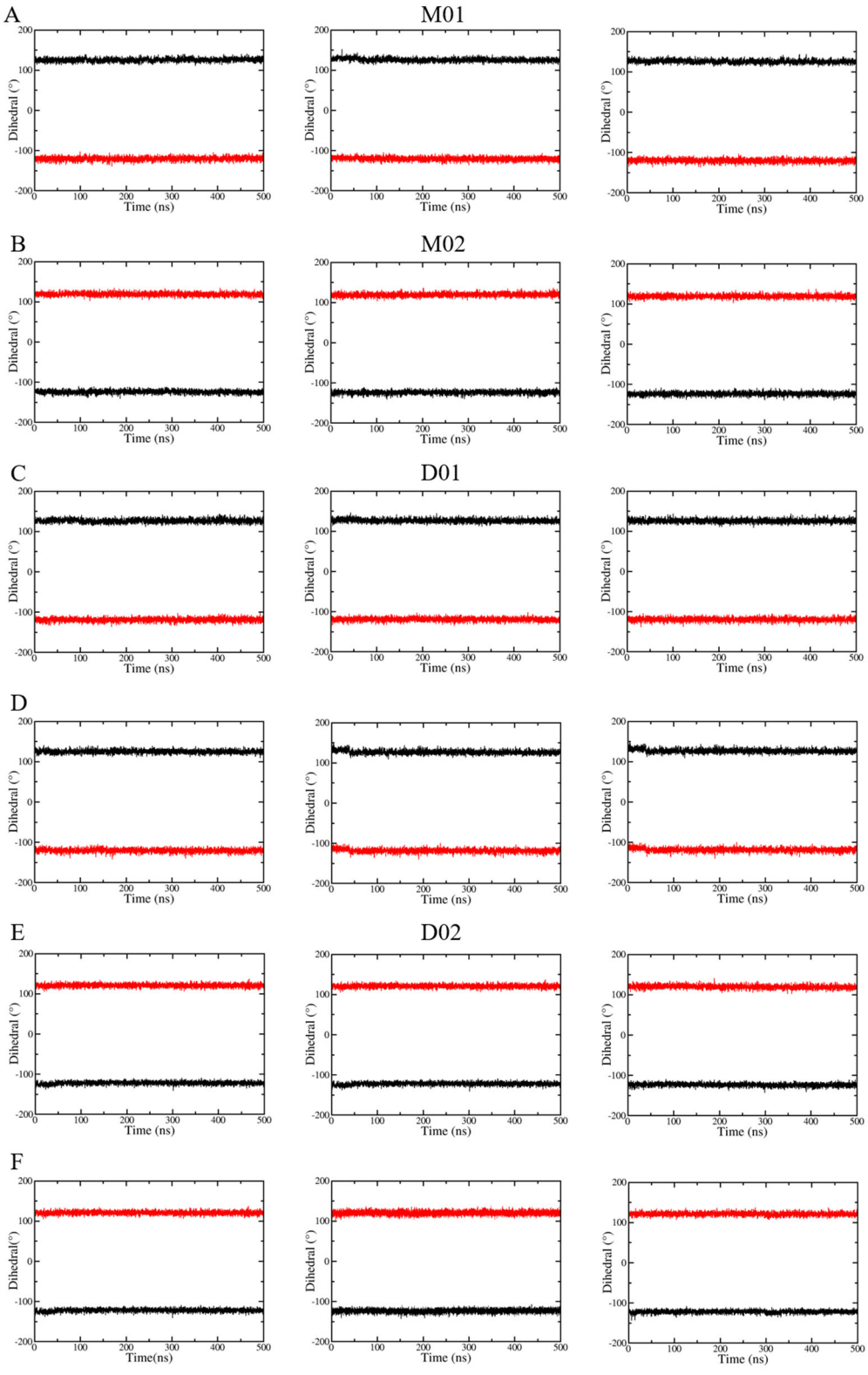

Figure S1. The variations of ligand dihedral angles along the simulation times. The black and red lines indicate the N-C-CA*-CB and N-C-CA-HA dihedral angles of glutamate group respectively for ligands **M01**, **M02**, **D01**, and **D02**.

Table S1. The physicochemical properties (calculated by RDKit) and ADMET analysis (predicted by ADMETlab 2.0, https://admetmesh.scbdd.com/) for all studied inhibitors.

	DCFPyL	**M01**	**M02**	**D01**	**D02**	**S01**	**S02**
Physicochemical properties							
Log P	-0.819	0.442	0.679	0.075	0.410	-0.132	-4.773
Mol. Wt.	442.150	521.110	521.110	866.230	866.230	1000.160	601.060
#HBA	12	14	14	25	25	26	12
#HBD	6	6	6	12	12	14	6
TPSA	195.020	225.500	225.500	407.630	407.630	422.460	199.200
ADMET							
PPB	23.896%	84.049%	85.517%	67.609%	69.920%	73.653%	77.497%
VD	0.368	0.332	0.256	0.812	0.692	0.741	0.413
Fu	59.594%	19.653%	16.699%	27.909%	22.620%	20.289%	11.837%
MDCK Permeability	15×10^{-6}	12×10^{-6}	4.6×10^{-6}	15×10^{-6}	4.8×10^{-6}	5.6×10^{-6}	140×10^{-6}
$T_{1/2}$	0.708	0.897	0.925	0.922	0.952	0.857	0.824
Bioconcentration Factors	-0.051	-0.053	-0.065	-0.355	-0.376	-0.062	0.181
IGC_{50}	2.407	2.695	2.636	2.564	2.474	3.305	3.116
$LC_{50}FM$	3.824	4.080	4.04	4.434	4.356	4.408	4.299
$LC_{50}DM$	2.803	2.908	2.957	1.846	1.944	2.266	4.004

Log P: Log of the octanol/water partition coefficient.

Mol. Wt.: Molecular weight. The unit is Da.

#HBA: Number of hydrogen bond acceptors.

#HBD: Number of hydrogen bond donors.

TPSA: Topological Polar surface Area. The unit is Å².

PPB: Plasma Protein Binding.

VD: Volume Distribution. The unit is L/kg.

Fu: The fraction unbound in plasms.

MDCK Permeability: The ability of substances to pass through MDCK cells. The unit is cm/s.

$T_{1/2}$: The output value is the probability of having long half-life.

Bioconcentration Factors: Bioconcentration factors are used for considering secondary poisoning potential and assessing risks to human health via the food chain. The unit is -log10[(mg/L)/(1000*MW)].

IGC_{50}: Tetrahymena pyriformis 50 percent growth inhibition concentration. The unit is -log10[(mg/L)/(1000*MW)].

$LC_{50}FM$: 96-hour fathead minnow 50 percent lethal concentration. The unit is - log10[(mg/L)/(1000*MW)].

$LC_{50}DM$: 48-hour daphnia magna 50 percent lethal concentration. The unit is - log10[(mg/L)/(1000*MW)].

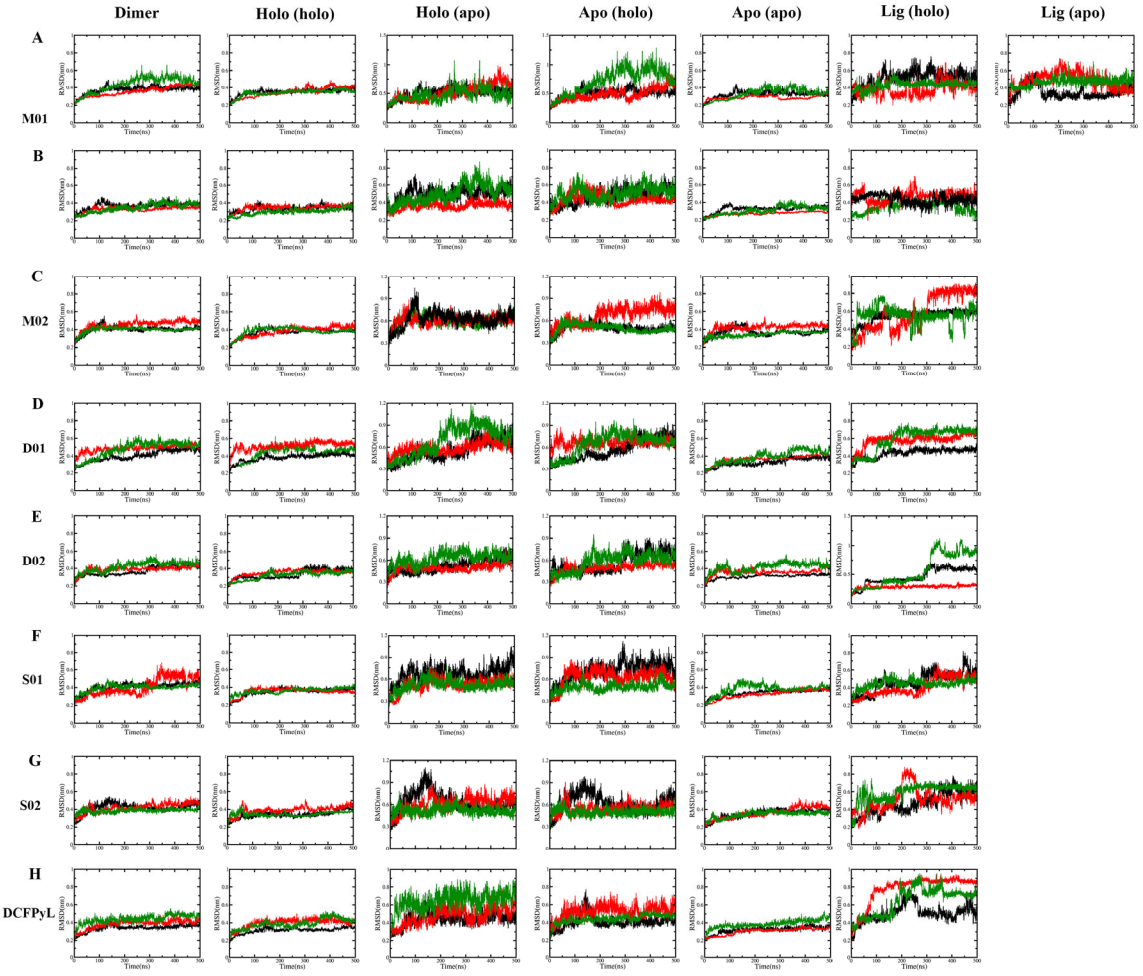

Figure S2. The stabilities of all PMSA-ligands in MD simulations. The RMSDs were calculated for Cα atoms of PMSA dimer (superimposed on all Cα atoms on both chains, noted as Dimer), Cα atoms of holo-monomer (superimposed on all Cα atoms of , noted as Chain A (fit A)), Cα atoms of holo-monomer (superimposed on all Cα atoms of chain B, noted as holo-monomer (fit apo-monomer)), Cα atoms of apo-monomer (superimposed on all Cα atoms of holo-monomer, noted as apo-monomer (fit holo-monomer)), Cα atoms of apo-monomer (superimposed on all Cα atoms of apo-monomer, noted as apo-monomer (fit apo-monomer)), heavy atoms of the ligand binding to holo-monomer (superimposed on all Cα atoms on holo-monomer, noted as LIG (holo-monomer)), and heavy atoms of the ligand binding to apo-monomer (superimposed on all Cα atoms of apo-monomer, noted as LIG (apo-monomer)). Different trajectories are represented by different colors (black, red, and green).

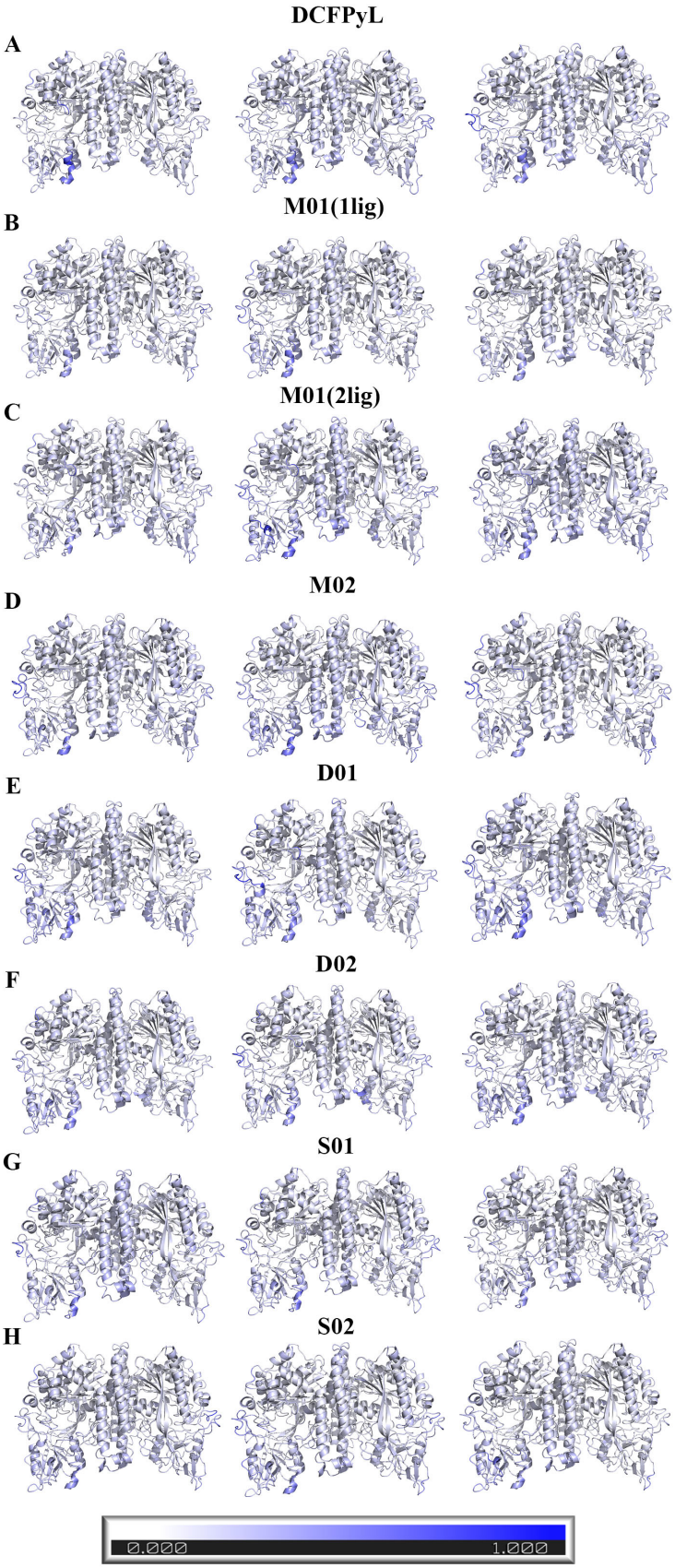

Figure S3. The RMSFs (in nm) of the PSMA dimers with different ligands, superposed on all Cα atoms.

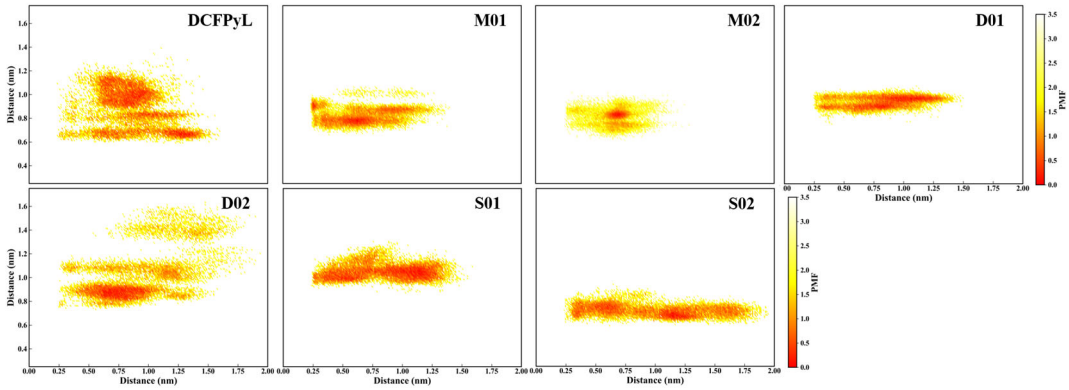

Figure S4. The potential of Mean Forces (PMFs in kcal/mol) of all systems, projected on the minimum distance of Phe546 and Tyr700 and the distance between the center of mass of the ligand and the Zn-binding group (ZBG). The PMF plots were calculated based on the conventional MD simulations. The distance was calculated using the GROMACS tool (gmx pairdist or gmx distance), then the entire range of distances was divided into two-dimensional bins with dimensions of 0.02 × 0.02 nm^2, finally the probability ($p_{i,j}$) of the number of data in each bin was calculated. The PMF was calculated according to the probability: $\mathrm{PMF}\ (\mathrm{i},\mathrm{j}) = -RT \times \ln p_{i,j}$.

Table S2. The clustering analysis results of all simulations. The clusters with a proportion larger than 0.1% are listed.

Tracers	DCFPyL	M01	M02	D01	D02	S01	S02
C1	68.89%	66.44%	60.69%	38.53%	65.65%	43.86%	42.47%
C2	22.92%	24.51%	19.97%	28.95%	15.85%	26.29%	21.08%
C3	5.90%	4.24%	12.21%	21.17%	12.40%	16.36%	17.39%
C4	1.33%	1.93%	3.35%	5.21%	4.70%	12.49%	7.44%
C5	0.69%	1.49%	2.21%	3.34%	1.07%	0.67%	5.66%
C6	0.14%	0.46%	1.18%	1.12%	0.17%	0.19%	2.31%
C7		0.39%	0.19%	0.57%		0.10%	1.39%
C8		0.29%	0.11%	0.56%			0.82%
C9		0.20%		0.21%			0.75%
C10				0.20%			0.27%

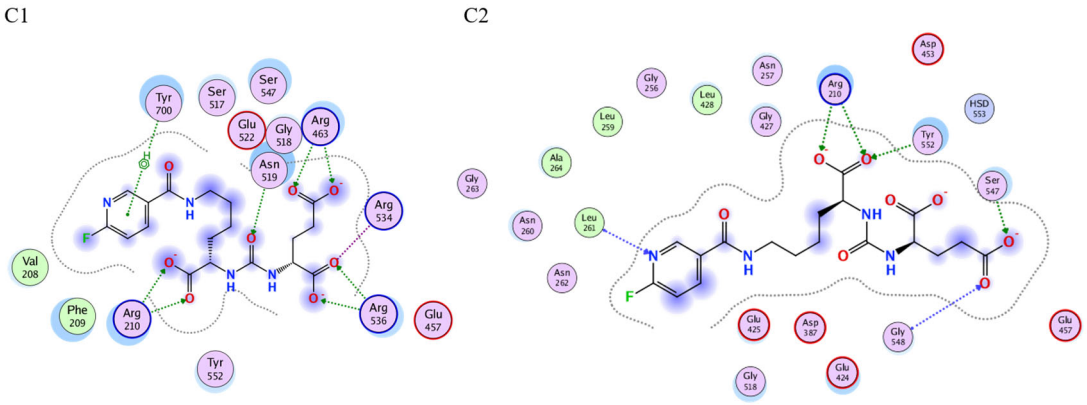

Figure S5. The PSMA-**DCFPyL** interactions of the representative conformations of the two largest clusters. The initial figures of protein-ligand interactions were generated from PoseEdit, an online platform for analysis of protein-ligand interactions (https://proteins.plus/), and then modified according to our simulation setting manually. It is the same for Figs S6-S11.

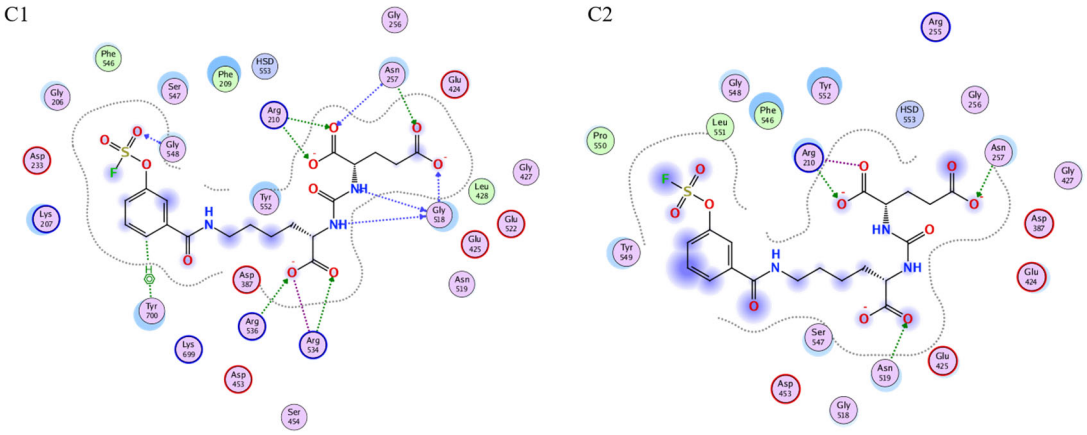

Figure S6. The PSMA-**M01** interactions of the representative conformations of the two largest clusters.

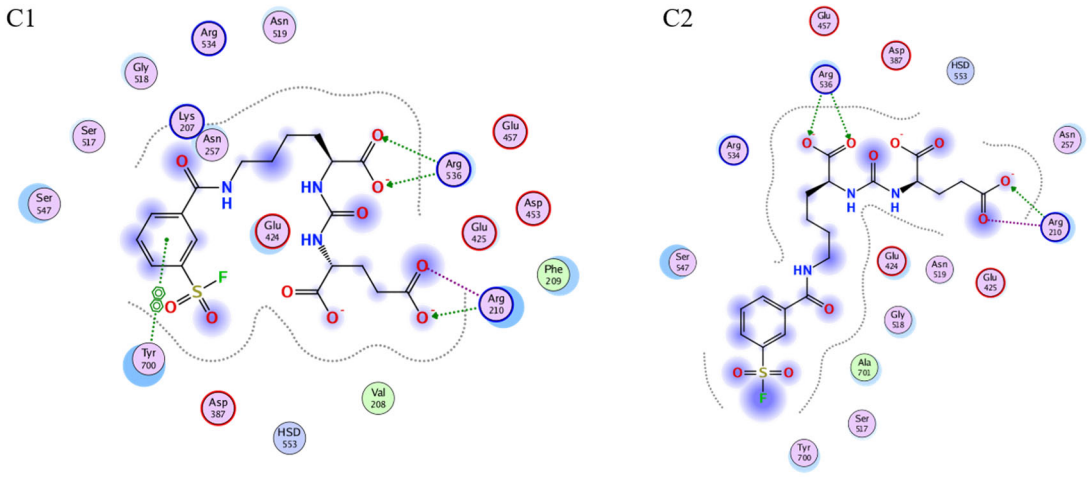

Figure S7. The PSMA-**M02** interactions of the representative conformations of the two largest clusters.

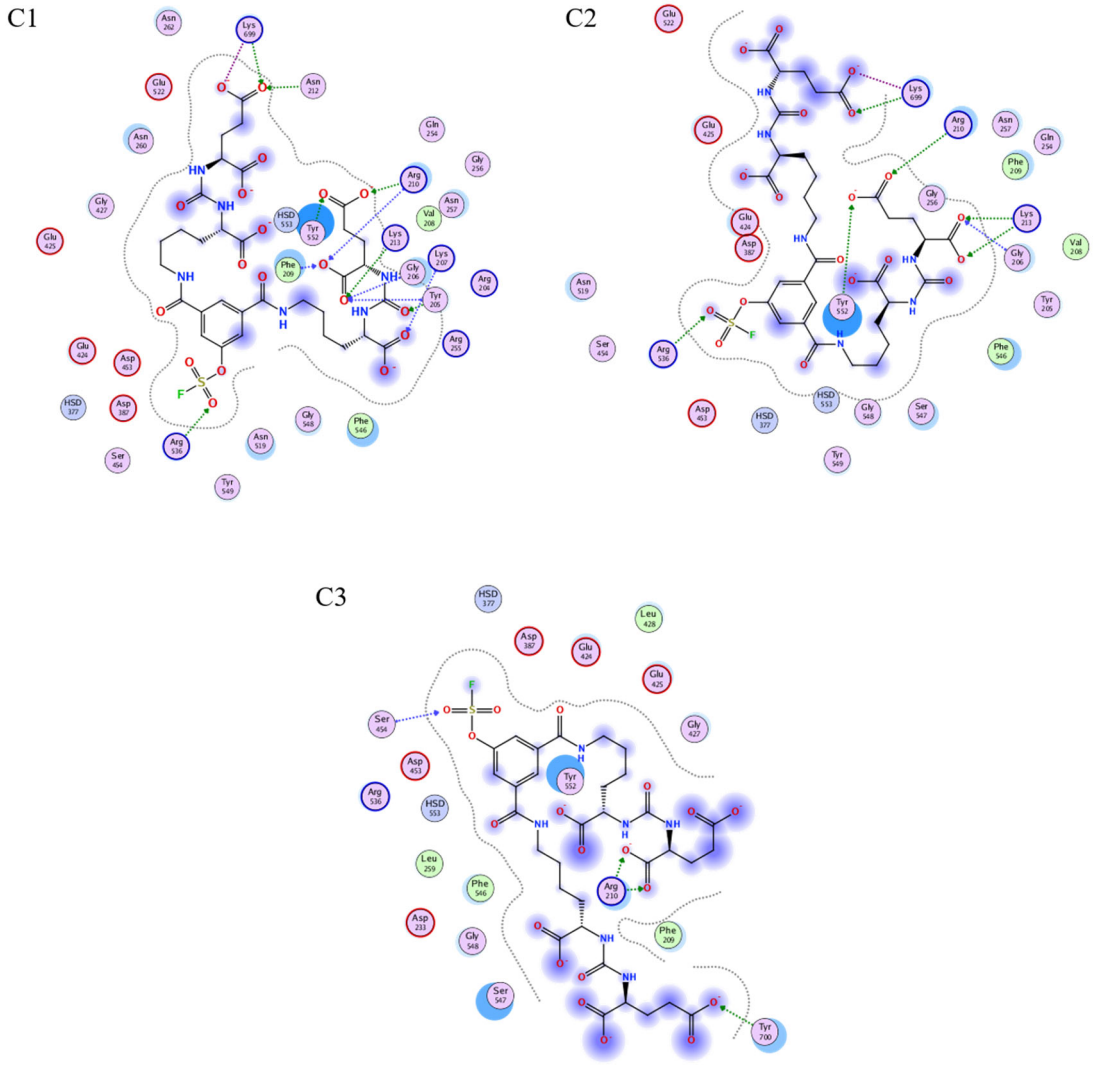

Figure S8. The PSMA-**D01** interactions of the representative conformations of the three largest clusters.

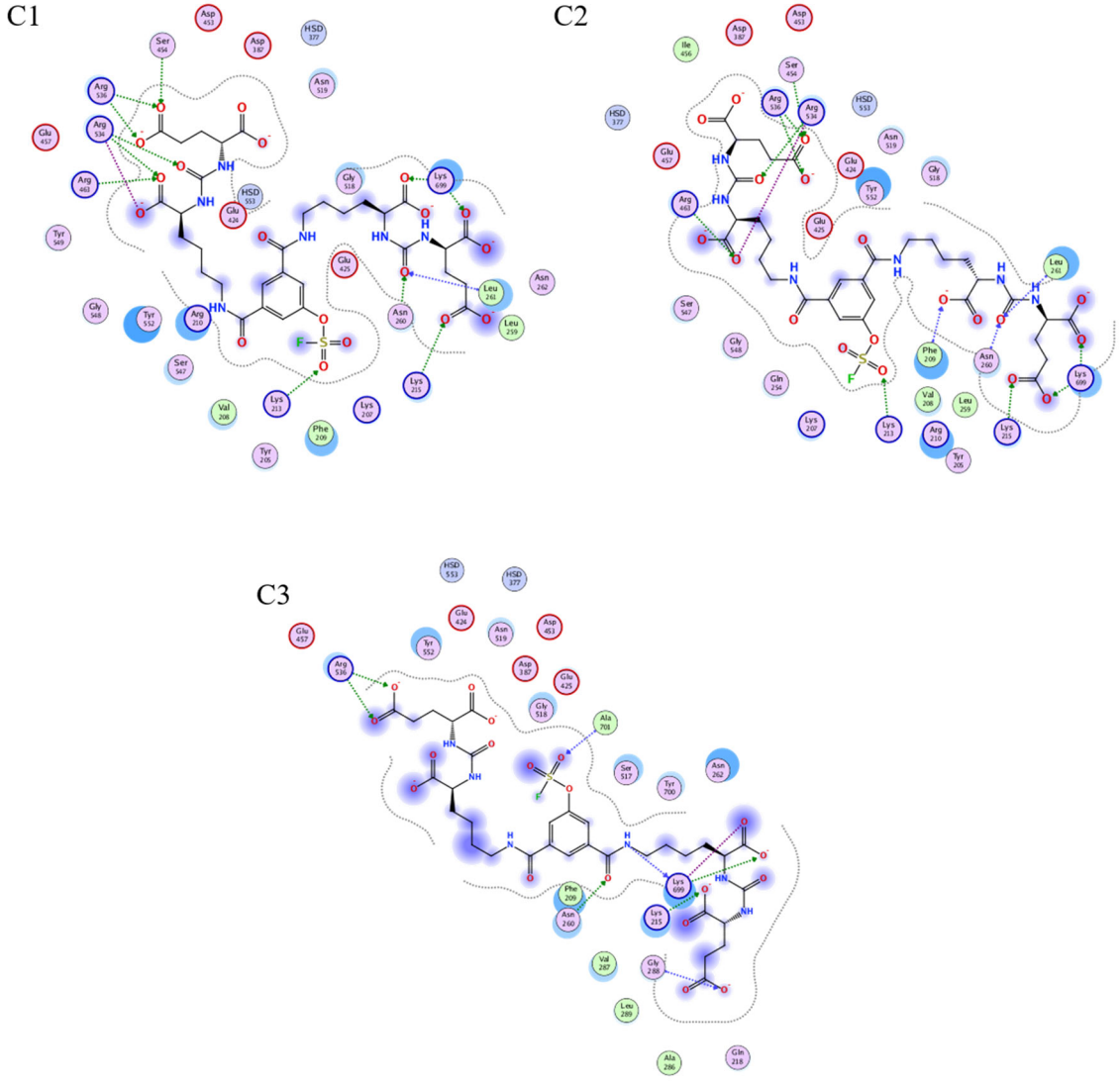

Figure S9. The PSMA-**D02** interactions of the representative conformations of the three largest clusters.

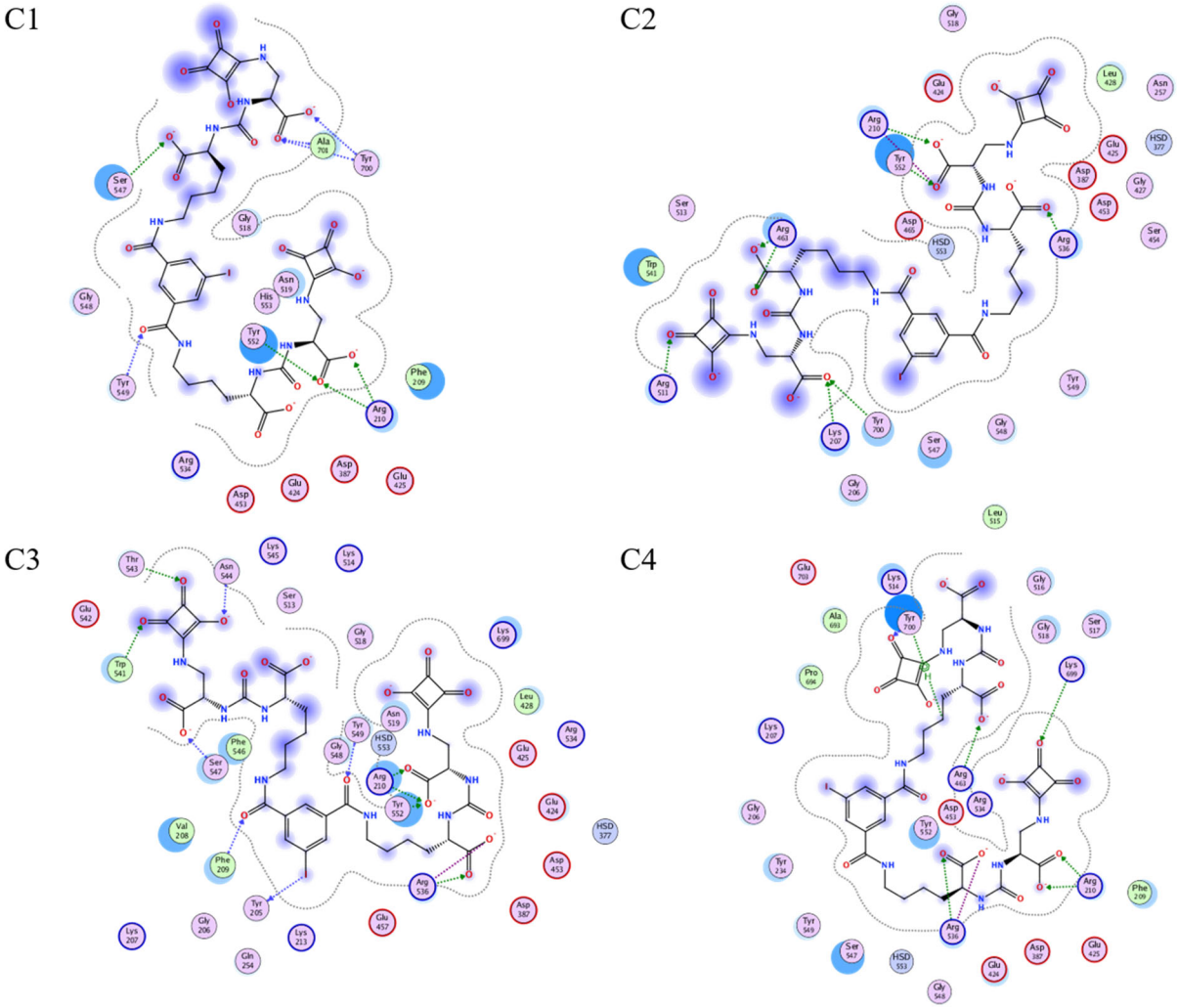

Figure S10. The PSMA-**S01** interactions of the representative conformations of the four largest clusters.

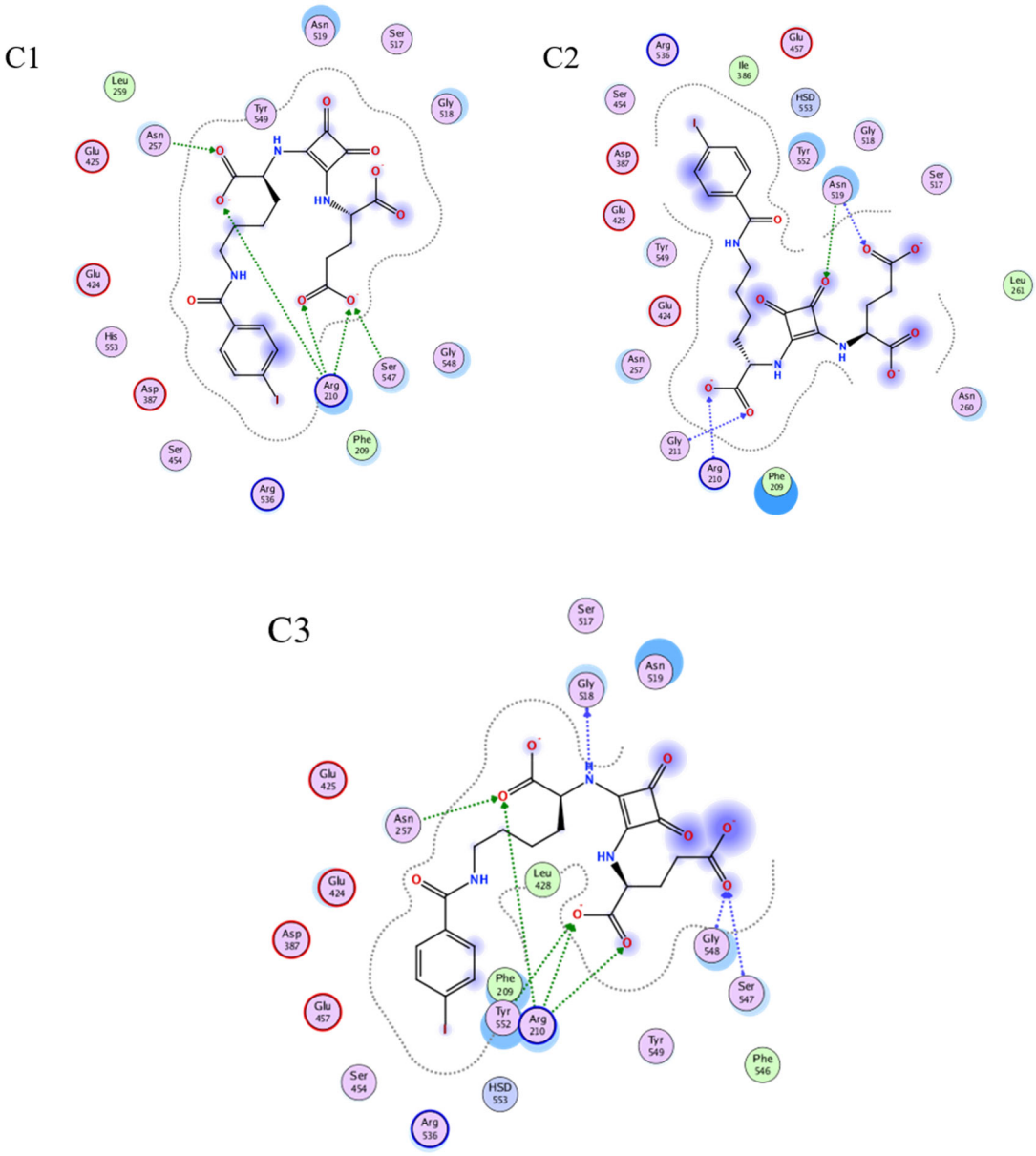

Figure S11. The PSMA-**S02** interactions of the representative conformations of the three largest clusters.

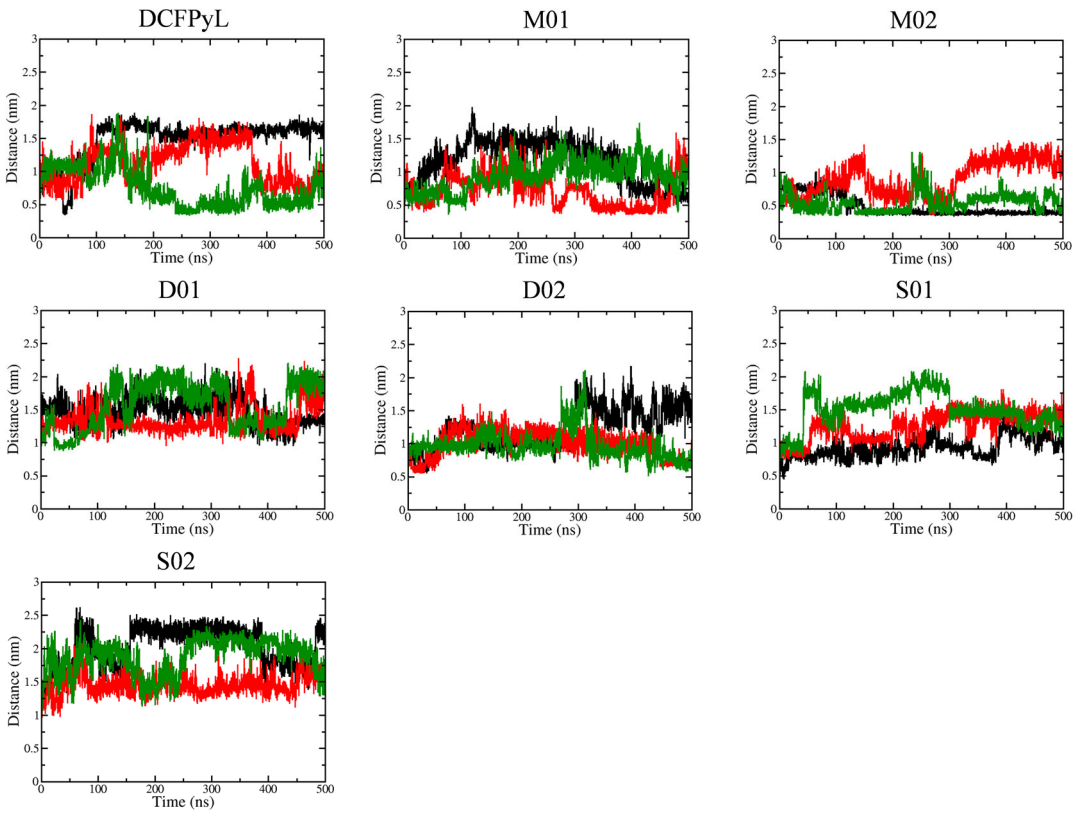

Figure S12. The evolutions of distances between the center of mass of the pyridine/benzene rings of ligands and Tyr700 along the simulation time. Different trajectories are represented by different colors.

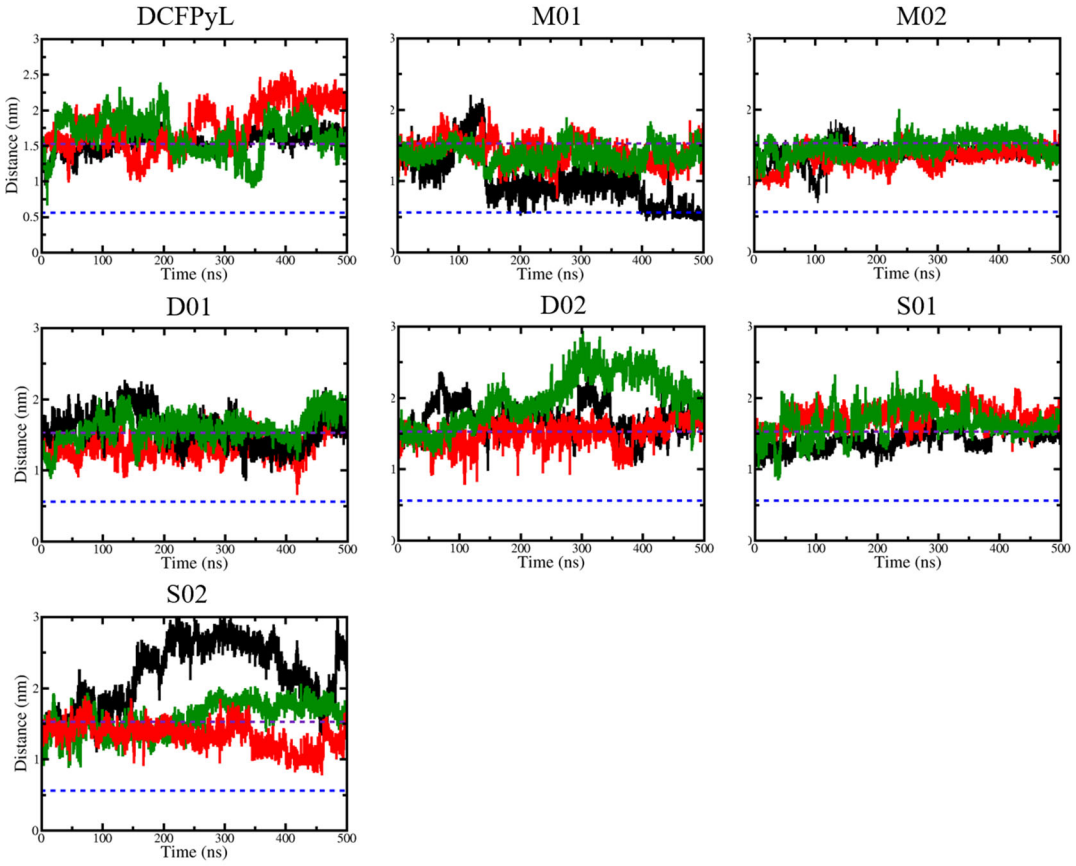

Figure S13. The evolutions of the distance between center of mass of Phe546 and Tyr700 along the simulation time. Different trajectories are represented by distinct colors. The distances in the open and closed states from the crystal structures are shown in black and blue dashed lines.

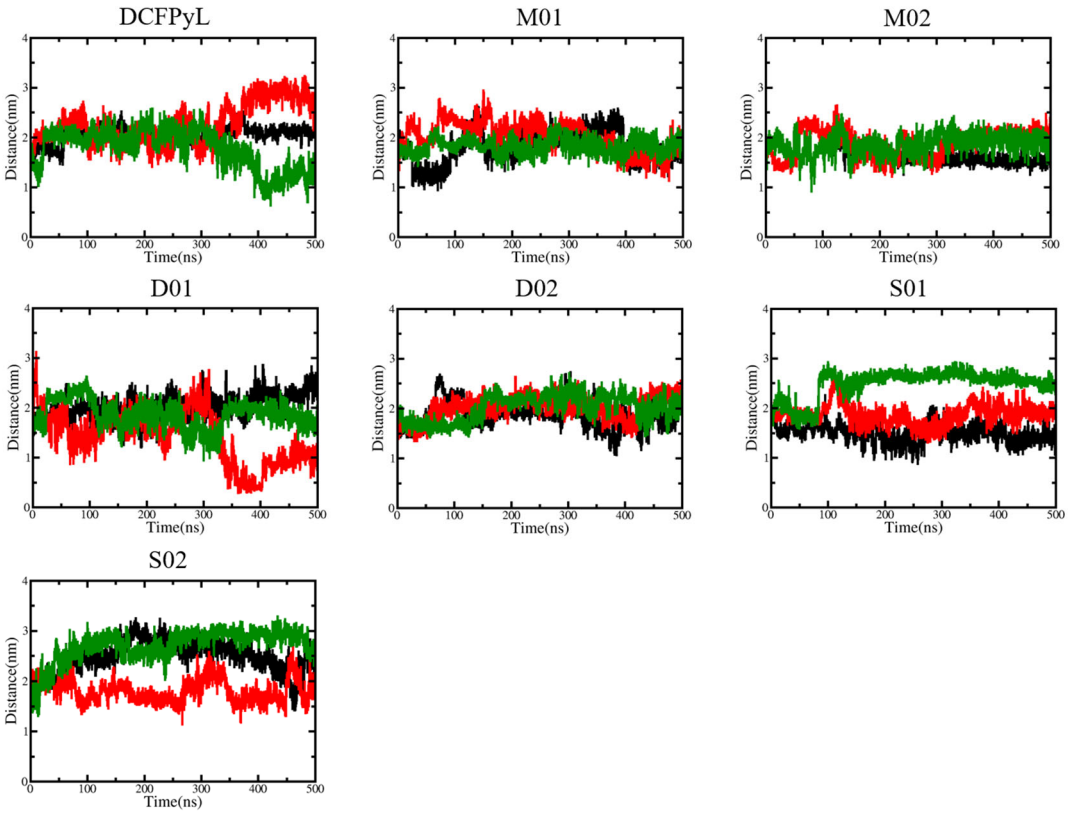

Figure S14. The evolutions of the minimum distances between the Interface Loop and Lys699 and Tyr700 in S1' pocket along the simulation time. Different trajectories are represented by distinct colors.

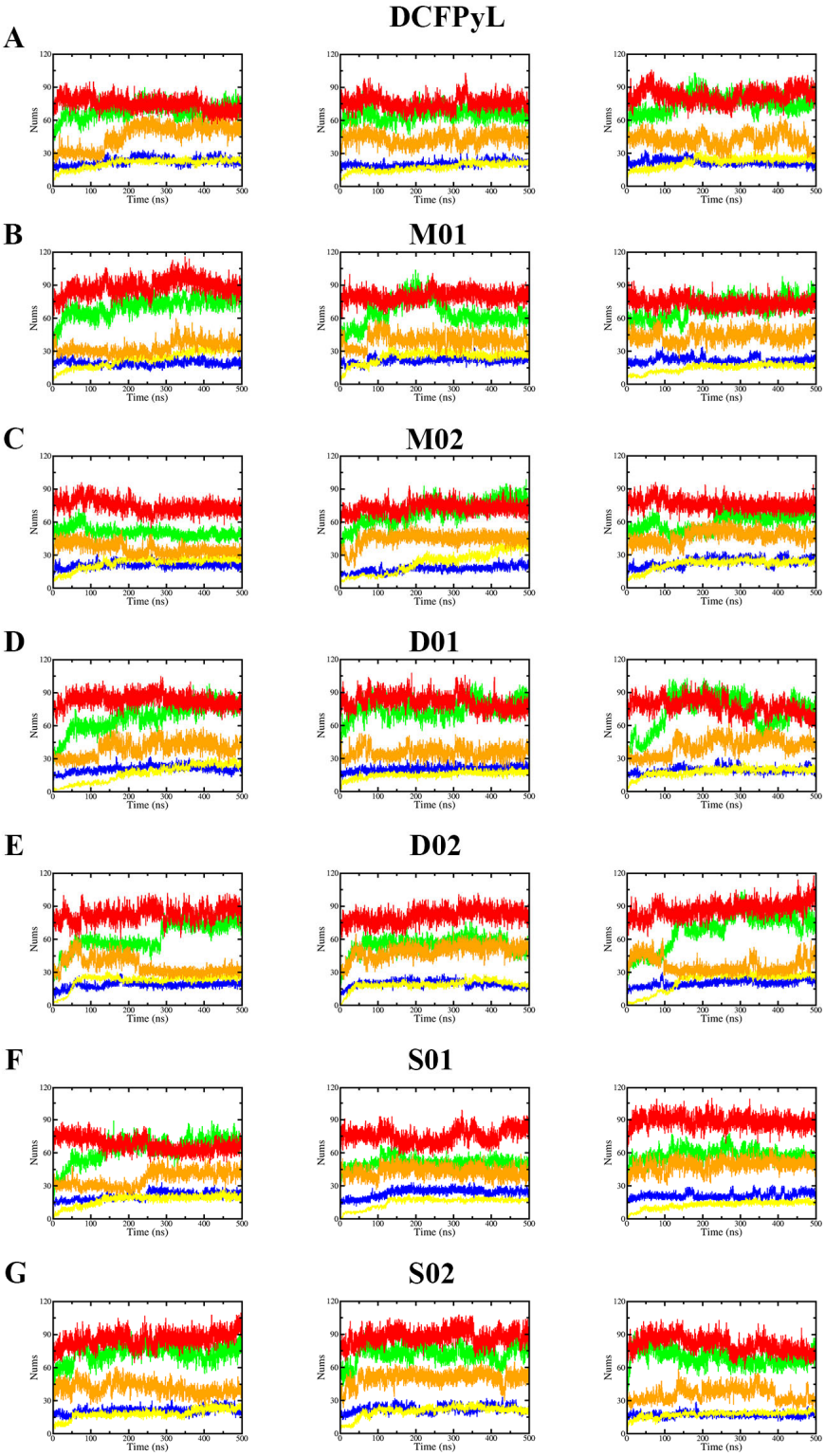

Figure S15. The variations in the number of water molecules within 0.35 nm of the structural elements of the binding pockets in the holo-monomer along the simulation times. Each column corresponds to a parallel trajectory. The S1' pockets are denoted in green, the Arg Patch in blue, the ZBG in yellow, the Arene-Binding Site (ABS) in orange, and the Entrance Lid, in red.

Table S3. The average (±variance) of the number of water molecules within 0.35 nm of the structural elements of the binding pockets in the holo-monomer.

	S1'	**Arg Patch**	**ZBG**	**ABS**	**Entrance Lid**
DCFPyL	69 (±8)	21 (±3)	20 (±5)	43 (±8)	77 (±7)
M01	67 (±10)	20 (±3)	20 (±7)	38 (±7)	80 (±8)
M02	59 (±11)	20 (±4)	22 (±7)	42 (±8)	75 (±6)
D01	71 (±13)	20 (±3)	16 (±6)	38 (±7)	80 (±7)
D02	61 (±14)	19 (±3)	21 (±7)	40 (±9)	83 (±7)
S01	57 (±9)	21 (±4)	15 (±5)	42 (±8)	77 (±11)
S02	71 (±8)	19 (±4)	18 (±4)	42 (±8)	84 (±8)